REGULATION OF THE CGAS-STING PATHWAY IN HEALTH AND DISEASE

APPROVED BY SUPERVISORY COMMITTEE

Nan Yan, Ph.D

Nicolai van Oers, Ph.D.

Zhijian Chen, Ph.D.

Nicholas Conrad, Ph.D.

DEDICATION

I would like to dedicate this thesis to my parents, Andrew and Elena Pokatayev.

REGULATION OF THE CGAS-STING PATHWAY IN HEALTH AND DISEASE

by

VLADISLAV ANDREYEVICH POKATAYEV

DISSERTATION / THESIS

Presented to the Faculty of the Graduate School of Biomedical Sciences

The University of Texas Southwestern Medical Center at Dallas

In Partial Fulfillment of the Requirements

For the Degree of

DOCTOR OF PHILOSOPHY

The University of Texas Southwestern Medical Center at Dallas

Dallas, Texas

December 2018

REGULATION OF THE CGAS-STING PATHWAY IN HEALTH AND DISEASE

Publication No. _____

Vladislav Andreyevich Pokatayev, Ph.D.

The University of Texas Southwestern Medical Center at Dallas, 2018

Supervising Professor: Nan Yan, Ph.D.

The innate immune system senses non-self or altered-self molecular structures through pattern recognition receptors in order to eliminate pathogens or damaged cells, and restore an organism to its basal physiology. Nearly all nucleated cell types can sense intracellular viral nucleic acids. These sensors detect either viral RNA through RIG-I like receptors or DNA through the cGAS-STING signaling pathway. Antiviral immune pathways are vital for resolution of viral infections; however, their dysregulation may give rise to various immune-mediated diseases.

The neuro-inflammatory autoimmune disease Aicardi-Goutières Syndrome (AGS) develops from mutations in genes encoding several nucleic acid processing proteins, including

RNase H2. Defective RNase H2 may induce accumulation of self-nucleic acid species which trigger chronic inflammation leading to AGS pathology. We created a knock-in mouse model with an RNase H2 AGS mutation in a highly conserved residue of the catalytic subunit, *Rnaseh2a*$^{G37S/G37S}$ (G37S), the most severe *Rnaseh2a* mutation categorized as it abolishes nuclease activity to less than 10% of WT RNase H2, to understand disease pathology. Importantly, I found that the G37S mutation induces a cellular anti-viral state, and an increased expression of interferon-stimulated genes dependent on the cGAS-STING signaling pathway. G37S homozygotes are perinatal lethal, and ablation of STING in G37S mice results in partial rescue of the perinatal lethality and complete rescue of the immune phenotype. This study motivates inhibitors of the cGAS-STING pathway in the goal of resolving *Rnaseh2a*-mediated AGS.

As my previous work implicates STING in the development of AGS, I performed a genetic screen to identify novel regulators of this protein. I discovered that TOLLIP, a protein previously identified as a regulator of extracellular Toll-like receptor pathways, can function as a positive regulator of the cGAS-STING pathway. TOLLIP antagonizes STING protein degradation through a regulatory pathway controlled by the protein IRE1α. In *Tollip*$^{-/-}$ cells, IRE1α is activated and induces lysomal-mediated degradation of STING. Chronic activation of this degradative pathway blunts the cellular response to cGAS or STING agonists. These findings have implications in vivo, as deleting *Tollip* in a mouse model for AGS, the *Trex1*$^{-/-}$ mouse, can rescue symptoms of the disease. These findings have clinical importance, as novel therapeutics against TOLLIP can be developed to treat auto-inflammation caused by dysregulation of the cGAS-STING signaling pathway.

TABLE OF CONTENTS

TABLE OF CONTENTS

PRIOR PUBLICATIONS

1. Pokatayev V., Hasin N., Chon H., Cerritelli S., Sakhuja K., Ward J., Morris H.D., Yan N., Crouch R.J. 2016. RNase H2 catalytic core mutant invokes cGAS-STING innate immune sensing pathway in mice. *The Journal of Experimental Medicine*. Vol 213(3): 329-336.

2. Starokadomskyy P., Gemelli T., Rios J., Xing C., Wang R., Li H., Pokatayev V., Dozmorov I., Khan S., Miyata N., Fraile G., Raj P., Xu Z., Xu Z., Ma L., Lin Z., Wang H., Yang Y., Amitai D.B., Orenstein N., Mussaffi H., Baselga E., Tadini G., Grunebaum E., Sarajlija A., Krzweski K., Wakeland E.K., Yan N., Morena M.T., Zinn A.R., Burstein E. 2016. DNA polymerase-α regulates type I interferon activation through cytosolic RNA:DNA synthesis. *Nature Immunology*. Vol 17(5): 495-504.

3. Pokatayev V., Yan N. 2017. Methods of Assessing STING Activation and Trafficking. Innate Antiviral Immunity. Methods in Molecular Biology. Vol 1656: 167-174.

4. Gonugunta V.K., Sakai T., Pokatayev V., Yang K., Wu J., Dobbs N., Yan N. 2017. Trafficking-mediated STING degradation requires direct sorting to acidified endolysosomes and can be therapeutically targeted to enhance anti-tumor response. *Cell Reports.* Vol 21(11): 3234-3242.

LIST OF FIGURES

CHAPTER ONE FIGURES

CHAPTER TWO FIGURES

CHAPTER THREE FIGURES

CHAPTER FOUR FIGURES

LIST OF TABLES

LIST OF DEFINITIONS

3-MA – 3-methyladenine

AKT – protein kinase B

AGS – Aicardi Goutières syndrome

ATP – adenosine triphosphate

BafA1 –bafilomycin a1

CARD – caspase activation and recruitment domain

cGAMP – cyclic guanosine monophosphate–adenosine monophosphate

cGAS – cyclic GMP-AMP synthase

CSF – cerebrospinal fluid

CTT – c-terminal tail

DAMP – danger associated molecular pattern

dsDNA – double-stranded deoxyribonucleic acid

dsRNA – double-stranded ribonucleic acid

ER – endoplasmic reticulum

ERGIC – endoplasmic reticulum-Golgi intermediate compartment

GTP – guanosine triphosphate

HD – Huntington's disease

IFN – interferon

IRF3 – interferon regulatory factor 3

IRF7 – interferon regulatory factor 7

ISG – interferon stimulated gene

LIST OF DEFINITIONS

LPS – lipopolysaccharide

MAVS – mitochondrial antiviral signaling protein

MDA5 – melanoma differentiation-associated protein 5

MyD88 – myeloid differentiation primary response 88

NF-κB – nuclear factor kappa-light-chain-enhancer of activated B cells

NTase – nucleotidyl-transferase

PAMP – pathogen associated molecular pattern

pDC – plasmacytoid dendritic cell

PKR – protein kinase R

PRR – pattern recognition receptor

PTM – post-translational modification

RIDD – regulated IRE1α-dependent decay

RIG-I – retinoic acid-inducible gene I

ssRNA – single-stranded ribonucleic acid

STING – stimulator of interferon genes

TBK1 – TANK-binding kinase I

Tg – thapsigargin

TLR – toll like receptor

TOLLIP – toll interacting protein

TRIF – TIR-domain-containing adapter-inducing interferon-β

UPR – unfolded protein response

CHAPTER ONE

INTRODUCTION

Innate Immunity

The dual branches of the immune system, the innate and adaptive, principally activate through receptor-mediated sensing of microbial molecular structures or antigens, respectively. Receptor recognition of either type of ligand leads to cellular reprogramming which occurs at genetic, biochemical, and organelle levels. These outputs vary depending on the stimuli and cell-type, but serve a common purpose of preventing infectious disease. Outputs occur in response to the sudden introduction of a stimulus, or when the amount of stimulus is elevated above a threshold that is determined by positive and negative regulators of these sensing systems (1). It can be generalized that both branches of the immune system are actively detecting molecular changes in the environment (2).

While both branches of the immune system sense ligands, temporal separation of this sensing is one major distinguishing feature between the two. The innate immune system is one of an organism's first lines of defense against pathogenic insults. Cellular germline-encoded proteins, known as pattern recognition receptors (PRRs), sense non-self molecular structures from microbes or viruses termed pathogen associated molecular patterns (PAMPs) (3). These sensors recognize ligands which are either extracellular or intracellular and this spatial separation can designate distinct cellular responses. In the case of any PRR, ligand recognition will instigate protein signaling cascades which culminate in the activation of various transcription factors regulating a diverse array of genes. PRR-induced genes are multi-faceted but often encode

immune cytokines, proteins which allow activation of other immune cells in the body, thereby leading to expansion of the innate immune response and eventual activation of the adaptive immune system. PRR-induced genes also encode proteins that have direct anti-microbial or anti-viral functions important in limiting pathogen replication (3).

Antiviral Immunity

Numerous PRRs exist to recognize unique molecular components of non-self origin (or PAMPs). As viruses are composed of protein capsules, mammalian cells have evolved to sense the encapsulated viral nucleic acids. PRRs recognize unique modifications or lack thereof on non-self nucleic acids or whenever nucleic acids are misplaced in cellular compartments, such as DNA in the cytosol (4). While extracellular or endosomal nucleic-acid sensing PRRs are limited largely to innate immune cell types, nearly all cell types express cytosolic PRRs that respond to intracellular insults from non-self nucleic acids and induce innate immune signaling (5).

Type I Interferons

A key cellular response that can be induced following the sensing of microbial or viral ligands is the type I interferon (IFN) response. Nearly all mammalian cell types can either produce or respond to type I IFNs. In humans there are 13 isoforms of IFNα proteins and 1 IFNβ protein (6). Type I IFN proteins can be released after activation of certain PRRs, and are induced by the transcription factors interferon regulatory factor 3 (IRF3) and 7 (IRF7). Secreted IFN proteins signal in a paracrine and autocrine manner through plasma membrane receptors, IFNAR1 and IFNAR2, and activate the JAK-STAT signaling pathway (Figure 1.1) (6).

Downstream of this pathway hundreds of genes referred to as interferon stimulated genes (ISGs) will be transcribed (7). Importantly, ISGs can also be activated directly by IRF3 and IRF7 in an IFN-independent manner (99). In contrast, ISG expression downstream of JAK-STAT pathway is regulated by IRF9 (7). ISGs have broad immune and non-immune functions; however, they are largely induced to inhibit viral replication in a cell-type and virus-specific manner. The type I IFN response is not associated with all PRRs, but is limited to those that have antiviral roles. The antiviral mechanism of ISGs, from individual antiviral function to systems level understanding of how they are coordinated during different viral infections, is an area of intense investigation (8).

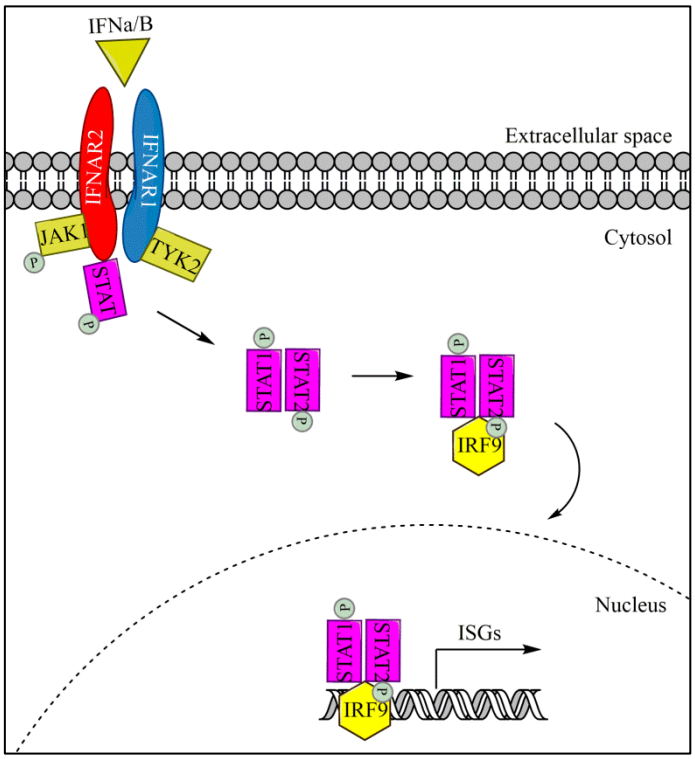

Figure 1.1: Type I IFN Signaling
A schematic of IFNα/β signaling through IFN receptor heterodimers IFNAR1 and IFNAR2. Cytokine binding instigates phosphorylation of JAK/STAT signaling to induce the activation of transcription factor IRF9. Nuclear IRF9 regulates the transcription of numerous antiviral genes termed ISGs which can render cells resistant to viral infections in virus- and replication step-dependent manners.

Toll-like Receptor Signaling

Toll-like receptors (TLRs) are among the first innate immune sensors characterized, and the first report was of TLR4 being the sensor of lipopolysaccharide (LPS), a constituent of the gram-negative bacterial cell wall (9). Shortly after that discovery, TLR3 was reported to be involved in the sensing of double-stranded RNA (dsRNA). TLR3 binds to dsRNA of at least 40

base-pairs length within endosomal compartments (5). Ligand binding initiates recruitment of the signaling adapter TIR-domain-containing adapter-inducing interferon-β (TRIF). TRIF allows for the activation of signaling kinase tank-binding kinase 1 (TBK1) which phosphorylates the transcription factor IRF3 to activate immune genes. TLR3 also activates transcription factor nuclear factor kappa-light-chain-enhancer of activated B cells (NFκB) to produce inflammatory cytokines as well (5).

While TLR3 senses dsRNA, TLR7 and TLR8 sense single-stranded RNA (ssRNA) that contains stretches of poly-U or poly-G regions (10, 11). TLR7 and TLR8 also bind to RNA that lacks a 2'-O-methyl group, a modification commonly found on self-RNAs, thereby discriminating non-self from self (10, 11). Such a modification has been shown to prevent sensing of mammalian tRNA (12).

TLR9 is involved in the sensing of unmethylated CpG dinucleotides found within DNA and also RNA:DNA hybrid species (13, 14). Like TLR7 and TLR8, TLR9 recruits the adapter protein myeloid differentiation primary response (MyD88) rather than TRIF in order for downstream signaling to occur (Figure 1.2). These four TLRs are limited in expression to certain cell types in humans, with TLR3 being found on various leukocytes and lymphocytes, TLR7 and TLR9 principally being on plasmacytoid dendritic cells (pDCs), while TLR8 is on myeloid cells (5).

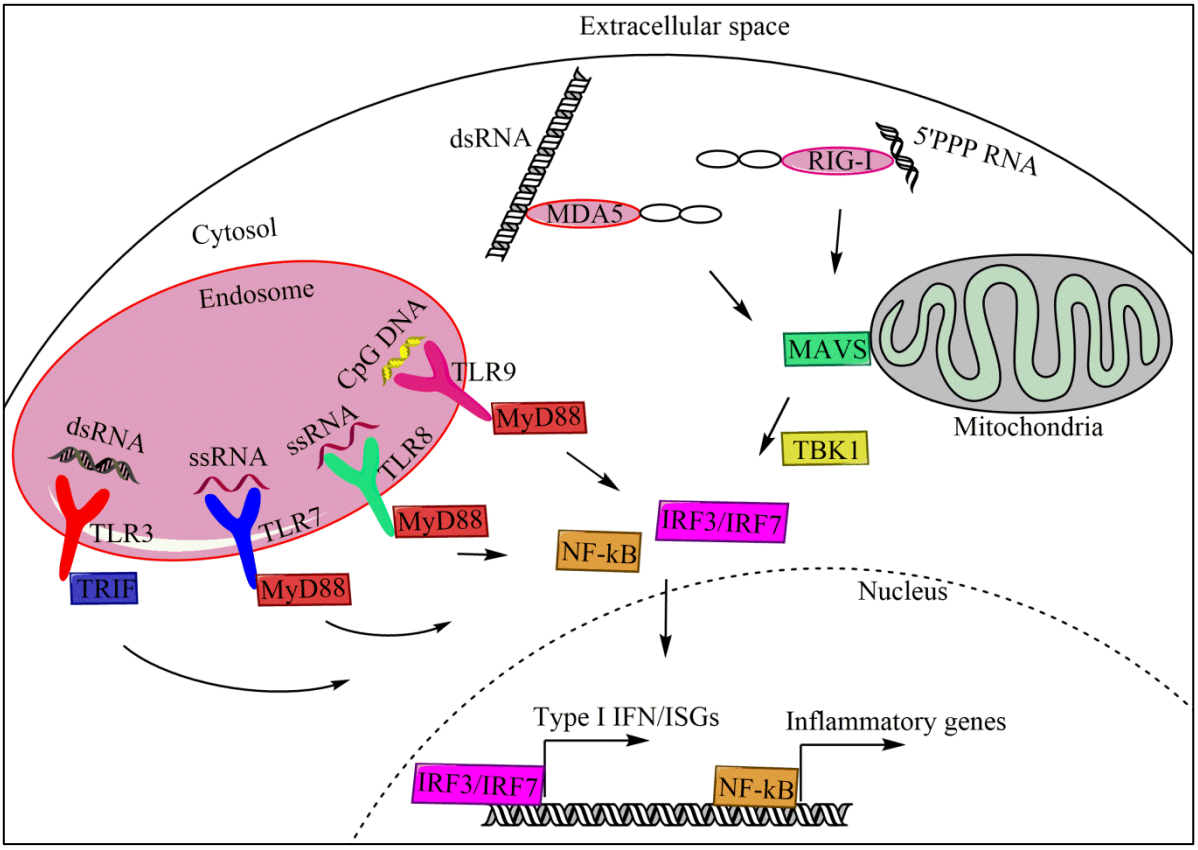

Figure 1.2: TLR and RLR Antiviral Immunity
A schematic of nucleic acid signaling through endosomal TLRs or intracellular RNA sensors, RIG-I and MDA5. Four separate endosomal TLRs mediate the recognition of diverse nucleic acids derived from viruses, prokaryotes or eukaryotic cells. These TLRs signal through either the MyD88 adaptor protein or TRIF to culminate in the production of type I IFNs or inflammatory genes. RIG-I and MDA5 function as sensors of RNA which is structurally distinct from mature cytosolic eukaryotic RNA. The two sensors differ in the types of RNA sensed, but both lead to production of type I IFNs and inflammatory genes.

RIG-I-like Receptor Signaling

As viruses replicate intracellularly, nearly all nucleated cell types have evolved to contain nucleic acid sensors in the cytosol. When viral RNA is introduced in the cytosol, the sensors retinoic acid-inducible gene I (RIG-I) or melanoma differentiation-associated protein 5 (MDA5) will bind to the RNA and become activated (Figure 1.2). Both sensors contain similar structural groups including an N-terminal caspase activation and recruitment domain (CARD), a C-

terminal domain involved in RNA binding, and a DExD/H RNA helicase domain which facilitates RNA binding (15). The sensors exist in an inactivated state; however binding of their cognate RNA ligands induces oligomerization which allows post-translational modifications on the sensors to occur, thereby initiating downstream signaling cascades (16).

RIG-I senses RNAs that are uncapped at the 5'-end and expose a triphosphate group. RIG-I senses short RNAs, and a minimum of 10 base pairs but less than 300 base pairs of a dsRNA moiety are sufficient for RIG-I activation (17). In contrast, MDA5 binds long stretches of viral dsRNA that are not found in mammalian cells, where several kilobase pairs mediate optimal activation of the protein (18). This RNA substrate specificity is largely determined by the preference of RIG-I binding to ends of RNA structures whereas MDA5 binds to grooves of the RNA helix. Following dsRNA binding, RIG-I and MDA5 undergo post-translational modifications (PTM) necessary for interaction with downstream signaling components. For example, polyubiquitination, the addition of multiple ubiquitin moieties, specifically K63-linked, is required for activation of RIG-I (19).

Activation of both RNA sensors leads to interaction with an essential adaptor protein, mitochondrial antiviral-signaling protein (MAVS). MAVS normally resides in an inactive state on the outer membrane of the mitochondrion, but undergoes phosphorylation after binding either RIG-I or MDA5. This phosphorylation at site S442 allows for the protein to further recruit TBK1 and activate downstream transcription factor IRF3 and type I IFN signaling (20).

cGAS-STING Signaling

In contrast to the differences in RNA composition between viruses and eukaryotes, intracellular sensing of DNA is dictated by the introduction of double-stranded DNA (dsDNA) into the cytosol, a compartment largely devoid of any DNA. The principal antiviral PRR against intracellular dsDNA is cyclic GMP-AMP synthase (cGAS) (Figure 1.3) (21, 22). cGAS contains a nucleotidyl-transferase (NTase) domain and a Mab21 domain (23). Normally the protein resides in an inactive state in the cytosol; binding of dsDNA longer than 21 base pairs induces dimerization of the protein and activation of the NTase domain (24). Activated cGAS utilizes adenosine triphosphate (ATP) and guanosine triphosphate (GTP) to synthesize a second messenger molecule called cyclic-guanosine monophosphate-adenosine monophosphate (2'3'-cGAMP) (25). cGAMP then diffuses throughout the cell and to neighboring cells through gap junctions, where it binds and activates a protein called stimulator of interferon genes (STING) (26). cGAS plays a pivotal role in the sensing of various DNA viruses, retroviruses, bacteria, as well as DNA of self-origin (27-30).

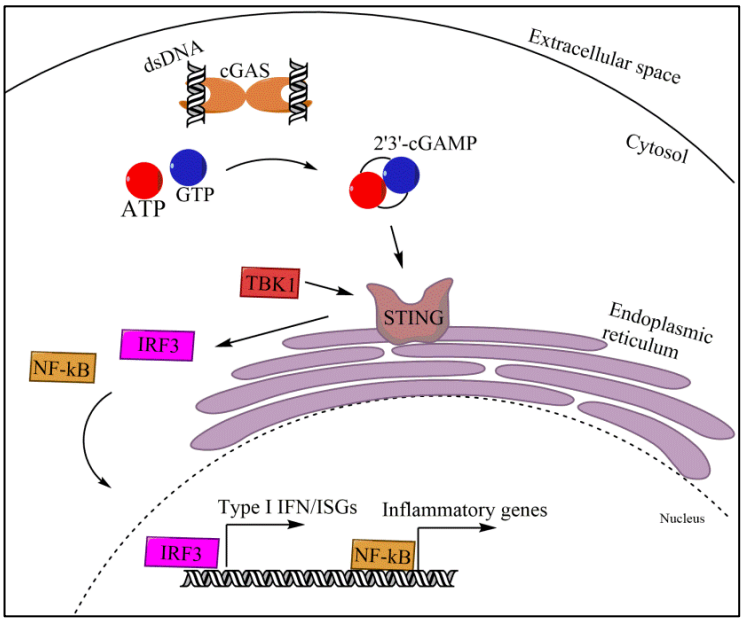

Figure 1.3: cGAS-STING Signaling
A model of intracellular DNA sensing by the cGAS-STING pathway. dsDNA-activated cGAS instigates conversion of ATP and GTP to a cyclic dinucleotide, 2'3'-cGAMP. This dinucleotide diffuses throughout the cell to activate STING, an adaptor protein and stand-alone sensor of cyclic dinucleotides. STING licenses transcription factor pathways IRF3 and NF-κB to enter the nucleus for immune gene expression.

STING is an endoplasmic reticulum (ER)-associated protein which normally resides in an inactive dimerized state. The introduction of bacterial cyclic-dinucleotides such as c-di-GMP and c-di-AMP, or mammalian cGAMP, is sensed by STING allowing for its activation (31). This dual sensing role designates onto STING roles as an adapter protein downstream of cGAS and also a stand-alone PRR for bacterial cyclic-dinucleotides. cGAMP binds to the STING C-terminus exposed to the cytosol and induces a structural change in the cytosolic domain. While definitive evidence is lacking, it is hypothesized this structural change allows for STING to begin trafficking from the ER to ER-Golgi intermediate compartments and then the Golgi apparatus (32). Along this trafficking route, and due to the structural change in STING, the signaling kinase TBK1 binds to and phosphorylates STING at residue S366 (20). This phosphorylation of STING then recruits IRF3 and allows for its phosphorylation and activation by TBK1. IRF3 will then translocate to the nucleus to activate type I IFNs and ISGs. The STING-TBK1 interaction also promotes NFκB activation; however the details regarding this mechanism are not well-characterized (33).

Following its trafficking route, STING co-localizes with LC3 puncta, cellular markers for autophagy (34); however, STING undergoes degradation through a lysosomal-mediated pathway, independent of canonical autophagy (35). This degradation is a means for cells to cease STING-mediated immune signaling, and also prevent STING-mediated cell death through lysosomal rupture (36). Without STING, cells are completely impaired in the response to cytosolic DNA and cyclic dinucleotides, highlighting its indispensable role in the innate immune response to microbial and viral infections.

Regulation of cGAS-STING Signaling

The output of immune signaling circuits is tightly controlled through regulation at each node of the circuit. This systems level regulation holds true for the cGAS-STING signaling pathway, as much work has illustrated key proteins which can positively or negatively regulate this pathway, thereby influencing the host response to infectious challenges while also limiting tissue damage caused by inflammation.

Regulation of cGAS

As the principal intracellular DNA sensor, cGAS is subjected to various post-translational modifications (PTM) which promote or inhibit its DNA-binding capability or enzymatic activity (Table 1). The first PTM on cGAS described was phosphorylation by protein kinase B (AKT) (37). Phosphorylation of cGAS residues S291 or S305 by AKT inhibits cGAS enzymatic activity and impairs DNA-mediated immune gene induction. Glutamylation of cGAS by TTLL4 and TTLL6 impairs its function by blocking cGAMP synthase activity and its DNA-binding ability, respectively (38). The protein TRIM38 carries out the sumoylation of cGAS; this PTM prevents basal cGAS degradation through a proteosomal-mediated pathway, thereby allowing optimal gene expression to occur (39). Finally, a key PTM involved in regulating the cGAS protein is ubiquitination, either the addition of single ubiquitin or poly-ubiquitin chains onto the protein. A variety of ubiquitinating or deubiquitinating enzymes have been identified. TRIM56 mediates the K335 monoubiquitination of cGAS (40). This modification enhances the ability of cGAS to dimerize in response to DNA, and potentiates the immune response. TRIM41 also mediates monoubiquitination of cGAS, and this is important for the intracellular DNA response; however

the mechanism of enhanced signaling remains unclear (41). The protein RNF185, in contrast to monoubiquitin, catalyzes addition of K27-linked polyubiquitin chains onto cGAS, which potentiates its cGAMP synthesis ability (42). USP14 is a deubiquitinating enzyme which counters the addition of K48-linked polyubiquitin chains onto cGAS, thereby preventing basal degradation through an autophagic pathway (43).

In addition to PTMs, cGAS has been reported to be regulated at the protein level through inflammasome-mediated cleavage of the protein. During inflammasome activation, cGAS is subjected to caspase-1 mediated cleavage at residues D140 and D157 (44). This cleavage leads to the loss of the protein and thereby a loss in the ability to respond to intracellular dsDNA challenge.

Table 1: cGAS PTMs

Regulation of cGAS				
Protein(s)	**PTM**	**Residue(s) Modified**	**Function**	**Ref**
AKT	Phosphorylation	S291, S305	Inhibits cGAS enzymatic activity	37
TRIM38	Sumoylation	K217, K464	Antagonizes basal proteosomal degradation of cGAS	39
TTLL4	Polyglutamylation	E302	Inhibits cGAS enzymatic activity	38
TTLL6	Polyglutamylation	E272	Impedes DNA binding	38
USP14	Deubiquitination	K414	Removes K48 ubiquitin chains to prevent basal autophagic degradation of cGAS	43
TRIM41	Monoubiquitination	*Unknown*	Promotes cGAS enzymatic activity	41
TRIM56	Monoubiquitination	K335	Enhances cGAS dimerization and downstream signaling	40
RNF185	Polyubiquitination	K173, K384	K27-linked chains promote cGAS enzymatic activity	42

Regulation of STING

As STING was identified prior to the discovery of cGAS, its regulation is more well characterized (Table 2). Similarly to cGAS, STING is subjected to several PTMs; among the

most important is phosphorylation. Following cGAMP binding, STING is subjected to phosphorylation by TBK1 at residue S366 (20). This phosphorylation is a key PTM as it allows recruitment and activation of transcription factor IRF3 and activation of IFN signaling.

Several ubiquitinating proteins have been identified which directly target STING as positive or negative regulators. Positive regulators of STING signaling through the addition of polyubiquitin chains include INSIG1, RNF26, TRIM32, and TRIM56 (45-48). These proteins either append K27-, or K63-polyubiquitin chains onto STING, and either maintain protein stability or promote other vital protein-protein interactions important for signal transduction. There also exist positive regulators which deubiquitinate STING to promote its signaling and these include EIF3S5, USP18 and USP20 (49, 50). These regulators all antagonize the basal addition of K48 polyubiquitin chains onto STING, thus preventing the protein from being degraded by the proteasome.

In contrast to positive regulators of STING, proteins which negatively regulate STING through polyubiquitination include RNF5, TRIM29, and TRIM30α (51-54). All three of these proteins catalyze the addition of K48-linked chains onto STING, thereby marking the protein for degradation through the proteasome. Only USP13 has been reported to negatively regulate STING through the removal of K27 polyubiquitin chains, a process which impairs TBK1 recruitment to STING (55). The interplay between all of these ubiquitin modifying enzymes is complex, and remains incompletely understood in terms of how they are coordinated in the basal and immune-challenged states to carry out STING signaling.

Several other PTMs on STING have been identified, albeit in less breadth as compared to ubiquitination. STING undergoes palmitoylation at the Golgi in order to activate TBK1 and

downstream immune genes (56). This modification occurs at residues C88 and C91, and mutation of these resides abolishes palmitoylation and impairs the STING-dependent immune response. The first described pharmacological inhibitor of STING directly targets this palmitoylation PTM and its application in vitro and in vivo abrogates STING-dependent signaling (57).

Similar to cGAS, sumoylation of STING also regulates its activity as this PTM prevents basal STING degradation through chaperone-mediated autophagy (CMA). TRIM38 sumoylates STING at K337 (39). This modification prevents its degradation by preventing recognition of a regulatory motif important in CMA. After STING activation, SENP2 desumolyates the protein, leading to STING degradation (39).

Table 2: STING PTMs

Regulation of STING				
Protein (s)	**PTM**	**Residue(s) Modified**	**Function**	**Ref**
AMFR/INSIG1	Polyubiquitination	K137, K150, K224, K236	Add K27-ubiquitin chains to recruit TBK1	45
RNF26	Polyubiquitination	K150	Antagonizes basal proteosomal degradation	46
TRIM32	Polyubiquitination	K20, K150, K224, K236	Adds K63-ubiquitin to promote TBK1 interaction	47
TRIM56	Polyubiquitination	K150	Adds K63-ubiquitin to induce dimerization	48
EIF3S5	Deubiquitination	*Unknown*	Removes K48-ubiquitin to prevent basal proteosomal degradation	49
USP18, USP20	Deubiquitination	*Unknown*	Removes K33/K48-ubiquitin to prevent basal degradation	50
RNF5	Polyubiquitination	K150	Adds K48-ubiquitin to induce proteosomal degradation	51
TRIM29	Polyubiquitination	K228, K370, K377	Adds K48-ubiquitin to induce proteosomal degradation	52
TRIM30α	Polyubiquitination	K275	Adds K48-ubiquitin to induce proteosomal degradation	53, 54
USP13	Deubiquitination	*Unknown*	Removes K27-linked ubiquitin chains to impair TBK1 recruitment	55
TBK1	Phosphorylation	S366	Recruit TBK1 and IRF3 to STING	20
Unknown	Palmitoylation	C88, C91	Allows assembly of multimeric complexes at Golgi	56
TRIM38	Sumoylation	K338	Antagonizes basal chaperone-mediated autophagy	39
SENP2	Desumoylation	K338	Promotes basal chaperone-mediated autophagy	39

Aicardi Goutières Syndrome

The regulation of innate immune signaling pathways is vital towards producing an optimal immune response against pathogens. The cost and benefit towards producing such a cellular response must be considered with the effects of inflammation on the host. Immune

responses against self-ligands must be prevented, and following resolution of infection, inflammation must cease in order to prevent tissue damage (58). As mentioned previously in the cGAS-STING signaling pathway, numerous regulatory mechanisms are in place to control inflammation following sensing of cytosolic DNA. Regulatory mechanisms such as PTMs are not unique to cGAS or STING, but exist in all innate immune signaling pathways. Regulation may occur at the PTM of immune signaling proteins, at transcriptional regulation of immune genes, or through the removal of immunogenic ligands released from cellular damage. If immune homeostasis is perturbed, such as when the host produces immune responses against self-ligands, auto-inflammation and/or autoimmune diseases such as Aicardi Goutières Syndrome (AGS) will occur.

Clinically described in 1984 by Jean Aicardi and Francoise Goutières, AGS was believed to arise from congenital viral infections (59). Patients characterized with the disease display brain calcification, high blood titers of IFNα protein, and growth retardation (60). It was years later determined that AGS is not caused by an infectious agent, but rather is a Mendelian auto-inflammatory and autoimmune disease. Due to a chronic elevation in type I IFN proteins in the blood and cerebral spinal fluid (CSF) of AGS patients, the disease is considered an interferonopathy. While clinical data in humans is lacking, it is believed that pathology in this disease arises from the destructive effects of type I IFN in host tissues, particularly the central nervous system (CNS) (59). Since the first genetic characterization of the disease in 2006, it is currently known that AGS arises from mutations in seven genes, with all genes encoding for proteins involved in either the degradation, modification, or the sensing of nucleic acids (Table 3) (59).

Trex1

TREX1 is a 3'-5' exonuclease whose primary function is to degrade self- or viral-DNA species within the cytosol (61). In 2006, mutations in the *Trex1* gene were identified in AGS patients (62). Currently there have been 33 mutations described within the *Trex1* gene which may give rise to AGS, with all mutations impairing the DNase activity of TREX1.

In *TREX1*-mutant associated AGS, self-DNA species from the nucleus will accumulate in the cytosol and become detectable by cGAS, leading to chronic activation of type I IFN signaling (63). In *Trex1*$^{-/-}$ mice, disease pathology can be rescued through genetic ablation of *Cgas* or *Tmem173* (STING) (64-67). It remains unclear the source of self-DNA which serves as a ligand for cGAS, with reports of endogenous retroviruses or DNA-damage induced nuclear debris serving as culprits (63, 68).

Samhd1

SAMHD1 is a dNTP triphosphohydrolase which depletes free dNTPs in the cell (69). This triphosphohydrolase is important in host-pathogen interactions, particularly with retroviral infections. SAMHD1 has been shown to be an HIV-1 restriction factor by prohibiting the virus from using cellular dNTPs during the reverse transcription step of the life cycle (70). SAMHD1 is itself induced by type I IFNs; therefore it is considered an ISG and has an evolutionarily important role in restricting retroviral infections (71).

The mouse model of *Samhd1*$^{-/-}$ does not exhibit overt inflammatory or autoimmune disease characteristics as seen in the *Trex1*$^{-/-}$ (72). The *Samhd1*$^{-/-}$ mouse exhibits slightly elevated ISGs as compared to *Samhd1*$^{+/+}$, while no signs of tissue pathology or autoimmunity are

observed. The elevation of ISGs in the *Samhd1*$^{-/-}$ mouse depends on the cGAS-STING pathway (73).

Similar to *TREX1*-mediated AGS, it remains unclear the source of endogenous nucleic acid which activates cGAS during *SAMHD1* deficiency. Endogenous retroviruses have been proposed as a source; however, more definitive evidence has implicated ssDNA genomic debris which arises from stalled replication forks (74). SAMHD1 has been shown to be recruited to these genomic regions to activate the DNase MRE11 and degrade stalled replication fork DNA. In the absence of SAMHD1, these ssDNA species accumulate intracellularly to activate cGAS. As cGAS is a dsDNA sensor, it is likely that ssDNA is sensed through spontaneous formation of dsDNA stem-loop regions; however definitive evidence is lacking (75). Importantly, this genomic repair function of SAMHD1 occurs independently of its dNTPase activity, therefore putting into question previous hypotheses on SAMHD1 controlling endogenous retroviral replication.

Adar1

ADAR1 is a dsRNA editing enzyme which converts adenosines to inosines through deamination (76). This editing ability leads to changes in molecular RNA processing events such as aberrant expression, splicing or degradation of RNA. There are two isoforms of ADAR1, p110 and p150 (77). These two isoforms differ in cellular localization, but it is the p150 isoform that is important in antiviral immunity and regulation of the innate immune response (78). In 2012, mutations in *Adar1* were reported in AGS patients (79). This report prompted the characterization of the *Adar1*$^{-/-}$ mouse whose early embryonic lethality has been known since

2004. ISG upregulation in the *Adar1*$^{-/-}$ mouse has been shown to entirely dependent on the MDA5-MAVS signaling pathway, while the lethality is only partially dependent, as *Adar1*$^{-/-}$ *MAVS*$^{-/-}$ mice succumb to death shortly after birth (78, 80, 81). This death in the double knockout animal is independent of ISGs or other antiviral signaling pathways, and the molecular mechanism remains unknown.

ADAR1 has also been implicated as a negative regulator of protein kinase R (PKR) (82). This regulation prevents PKR from sensing endogenous RNA and causing translational arrest. These findings highlight the importance of AGS proteins in non-immune mediated functions, and suggest non-immune mediated pathology in the development of AGS. It is unknown whether this PKR activation may cause the lethality observed in *Adar1*$^{-/-}$ *MAVS*$^{-/-}$ mice.

Ifih1

Ifih1 encodes for the dsRNA sensor MDA5 which senses long dsRNA ligands. In 2014, AGS mutations in *Ifih1* were reported (83). This report suggested the MDA5-associated AGS mutations are gain-of-function in which MDA5 is activated independently of ligand-binding. In vitro, these mutations lead to activation of the MDA5-MAVS pathway and production of inflammatory cytokines associated with AGS. Since this initial report, it has been demonstrated that the MDA5-associated AGS mutants respond to self-cellular nucleic acids, specifically in response to endogenous retroelements called Alu elements (84). The MDA5-associated AGS mutants lead to a conformational change in the RNA sensor which alters its sensitivity to Alu elements in the cellular cytosol, thereby allowing greater sensitivity in their recognition. While

the answer regarding the ligands and immune pathways in this AGS subtype has been addressed in vitro, in vivo studies are lacking.

Rnaseh2

RNASEH2 is a heterotrimeric protein composed of three subunits RNASEH2A, RNASEH2B, and RNASEH2C (85). It belongs to the RNase H family of proteins which are found in every organism in all kingdom of life, including even retroviruses (85). RNASEH2 performs two enzymatic activities: the cleavage of single ribonucleotides within a DNA duplex, and the cleavage of long stretches of RNA annealed to DNA, structures termed RNA:DNA hybrids. AGS mutations in the *Rnaseh2* subunit genes have been observed as early as 2006, with all mutants leading to a loss of function in the protein's enzymatic activity, either through direct impairment of ribonucleotide catalysis or through loss of protein expression (86).

In vivo studies of RNASEH2-mutant mediated AGS have not uncovered the etiology of disease. Previous studies have generated knockouts of the *Rnaseh2b* and *Rnaseh2c* genes (87, 88). These mice succumb to early embryonic lethality at day E9.5. Cells derived from these embryos display no upregulation in ISGs, nor do they express inflammatory cytokines. Importantly, however, these studies have largely determined that complete knockouts of RNASEH2 lead to a lethal DNA damage response which can only partially rescued to E11 with a cross onto $p53^{-/-}$. These partially rescued embryos also do not exhibit upregulation of ISGs; therefore molecular and genetic studies in vivo regarding the immune pathways active in RNASEH2 deficiency have been elusive.

As RNASEH2-mutant mediated AGS represents over half of the total AGS patients and with some subunit mutations manifesting the most severe clinical presentations of the disease,

the understanding of disease etiology is paramount. I sought out to understand this disease through the use of an *Rnaseh2a* mutant knock-in mouse model to molecularly and genetically define disease manifestation.

Table 3: Basis of AGS

Aicardi Goutières Syndrome			
Gene	**% AGS Patients**	**Active Immune Pathways**	**Ref**
Trex1	23%	cGAS-STING	64-67
Samhd1	13%	cGAS-STING	73
Adar1	7%	MDA5-MAVS	78, 80, 81
Ifih1	3%	MDA5-MAVS	83
Rnaseh2a, Rnaseh2b, Rnaseh2c	54%	cGAS-STING	Published work in Chapter 2

CHAPTER TWO

RNASE H2 CATALYTIC CORE AICARDI-GOUTIÈRES SYNDROME-RELATED MUTANT INVOKES CGAS-STING INNATE IMMUNE SENSING PATHWAY IN MICE

This chapter is a modification of the published article - RNase H2 catalytic core Aicardi-Goutières syndrome–related mutant invokes cGAS-STING innate immune sensing pathway in mice. *Journal of Experimental Medicine* February 15, 2016

Introduction

RNase H2 provides the main RNase H activity in humans (85) and is essential for removing ribonucleotides incorporated in genomic DNA during replication, as well as for resolving R-loops formed during transcription (87, 89, 90). The crystal structures of human and mouse RNase H2 revealed the interactions of the subunits and the positions of the more than 50 known AGS-related mutations in the three subunits (91, 92). Some mutations are located near the catalytic center and affect catalysis, whereas others affect stability or alter protein interactions. The most common mutations reported in AGS patients are found in the B subunit (60) and are associated with less severe disease phenotype than mutations in the catalytic A subunit. A mutation in a highly conserved glycine (G37S) near the catalytic center on the RNase H2A subunit causes a severe early onset presentation of AGS, likely as a result of a substantial loss of RNase H activity (86). Many in vitro studies showed that Serine substitution for Glycine 37 in RNases H2 of eukaryotes reduces RNase activity (86, 93-95). Mouse models using deletions of RNASE2B and RNASEH2C exhibit significant DNA damage, resulting in embryonic lethality at E9.5 (87, 88). These mice have elucidated important information on the role of RNase H2 in

genome stability, but because of their early death, have not yielded insight into the innate immune pathways responsible for disease manifestation. Likewise, neither do mice with residual levels of RNase H2B (R2B KOF [88]). Therefore, it remains unclear how RNASEH2 mutations lead to the development of AGS.

Experimental Procedure

Mice, cells, and viruses. G37S mice were generated by introducing the human disease associated point mutation into the conserved residue of mouse *Rnaseh2a* gene. *Ifnar1*$^{-/-}$ and *Rag2*$^{-/-}$ mice were obtained from Taconic Biosciences. *p53*$^{-/-}$ mice were obtained from The Jackson Laboratory *Mavs*$^{-/-}$ and *cGAS*$^{-/-}$ mice were obtained from Z. Chen (University of Texas Southwestern Medical Center, Dallas, TX) and *Tmem173*$^{-/-}$ mice were obtained from G. Barber (University of Miami, Miami, FL). Primary MEFs were isolated from embryos of indicated embryonic dates. These cells were maintained in DMEM with 20% (vol/vol) heat-inactivated FCS, 2 mM l-glutamine, 10 mM Hepes, and 1 mM sodium pyruvate (complete DMEM) with the addition of 100 U/ml penicillin and 100 mg/ml streptomycin and were cultured at 37°C with 5% CO2. VSV-PeGFP is a gift from A. Pattnaik (University of Nebraska, Lincoln, NE). Cells were plated overnight and, the next day, infected overnight with VSV-GFP at a multiplicity of infection of 1. Cells were washed with PBS before standard fixation with 4% paraformaldehyde in PBS (Affymetrix). Percentage of infectivity was assessed with FACS Calibur (BD). For viral RNA measurement, total RNA was extracted at various time points after infection, and VSV-G and -M RNA were measured with specific primers (96). Experiments performed in BSL-2 conditions were approved by the Environmental Health and Safety Committee at University of

Texas Southwestern Medical Center. Experiments involving mouse materials were approved by the Institutional Animal Care and Use Committees of the University of Texas Southwestern Medical Center and the National Institute for Child Health and Human Development (Bethesda, MD).

RNA isolation and quantitative RT-PCR. Total RNA was isolated with TRI reagent according to the manufacturer's protocol (Sigma-Aldrich), and cDNA was synthesized with iScript cDNA synthesis kit (Bio-Rad Laboratories). iTaq Universal SYBR Green Supermix (Bio-Rad Laboratories) and an ABI-7500 Fast Real-Time PCR system (Applied Biosystems) were used for quantitative RT-PCR analysis. RNA-seq was performed as previously described (96).

Table 4: RT-PCR oligos

Oligo	**Sequence (5'-3')**
Cgas Fwd:	ACGAGAGCCGTTTTATCTCGTACCC
Cgas Rev:	TGTCCGGAAGATTCACAGCATGTTT
Sting Fwd:	TCAGTGGTGCAGGGAGCCGA
Sting Rev:	CGCCTGCTGGCTGTCCGTTC
Mavs Fwd:	CCTCCGGGGACCTCACTCCG
Mavs Rev:	TGGGGACTCTGGTGGCTGGG
Tbk1 Fwd:	CCAGTGGATGTTCAAATGAGAGAAT
Tbk1 Rev:	TCTAGAACAGTGTATAAACTCCCAC
Cxcl10 Fwd:	GGGATCCCTCTCGCAAGGACGGTCC
Cxcl10 Rev:	ACGCTTTCATTAAATTCTTGATGGT
Ifit1 Fwd:	ACGCTTTCATTAAATTCTTGATGGT
Ifit1 Rev:	TGCTCAGCTGCTCGCTCTGGATCAA
Rsad2 Fwd:	AACCTGCTCATCGAAGCTGT
Rsad2 Rev:	ATAGTGAGCAATGGCAGCCT
Ifit3 Fwd:	TGGCCTACATAAAGCACCTAGATGG
Ifit3 Rev:	CGCAAACTTTTGGCAAACTTGTCT
Line1 Utr Fwd:	GGCGAAAGGCAAACGTAAGA
Line1 Utr Rev:	GGAGTGCTGCGTTCTGATGA
Line1 Orf2 Fwd:	GGAGGGACATTTCATTCTCATCA
Line 1 Orf2 Rev:	GCTGCTCTTGTATTTGGAGCATAGA

cGAMP activity bioassay. cGAMP activity in MEFs was measured by a co-culture bioassay as previously described (66). In brief, 2×10^5 human fibroblasts/ml were plated overnight. After attachment, 4×10^5 primary murine fibroblasts/ml were plated onto the human cells, with or without 200 mM CBX (Sigma-Aldrich) treatment or with separation by 0.4-μm polycarbonate trans-well inserts (Corning) for 18 h. Subsequent analysis was performed using a human-specific PrimePCR Array plate (Bio-Rad Laboratories).

shRNA knockdown and TBK1 inhibitor. shRNA oligos were synthesized (Sigma-Aldrich) and cloned into a pLKO.1-TRC cloning vector following Addgene's protocol. Lentiviral particles were packaged in HEK-293T cells and filtered with Amicon Ultra-15 centrifugal filters (EMD Millipore). shRNA-harboring lentiviruses were allowed to infect cells overnight with polybrene (10 μg/ml) treatment, and cells expressing the shRNA were selected with a puromycin concentration (Life Technologies) for several days. Puromycin selection was removed several days before subsequent analysis. For TBK1 inhibitor experiments, cells were treated with DMSO (% vol/vol) or 10 μM BX795 (Invivo-Gen) for 6 h. Cells were then washed with PBS and grown in DMEM with 20% FCS alone for several hours before subsequent analysis.

Table 5: shRNA oligos

Oligo	Sequence (5'-3')
Sh-Control (Luciferase) sense	CCGGAACTTACGCTGAGTACTTCGACTCGAGTCGAAGTACTC AGCGTAAGTTTTTTTG
Sh-Control (Luciferase) as	AATTCAAAAAAACTTACGCTGAGTACTTCGACTCGAGTCGAA GTACTCAGCGTAAGTT
Sh-mcGAS sense	CCGGAGGATTGAGCTACAAGAATATCTCGAGATATTCTTGTA GCTCAATCCTTTTTTG
Sh-mcGAS as	AATTCAAAAAAGGATTGAGCTACAAGAATATCTCGAGATATT CTTGTAGCTCAATCCT
Sh-mSting sense	CCGGCAACATTCGATTCCGAGATATCTCGAGATATCTCGGAAT CGAATGTTGTTTTTG
Sh-mSting as	AATTCAAAAACAACATTCGATTCCGAGATATCTCGAGATATCT CGGAATCGAATGTTG
Sh-mTBK 1 sense	CCGGCCAGAATCAGAATTTCTCATTCTCGAGAATGAGAAATT CTGATTCTGGTTTTTG
Sh-mTBK 1 as	AATTCAAAAACCAGAATCAGAATTTCTCATTCTCGAGAATGA GAAATTCTGATTCTGG
Sh-mMavs sense	CCGGGCTCTTTGATACCCTCTCCTACTCGAGTAGGAGAGGGTA TCAAAGAGCTTTTTG
Sh-mMavs as	AATTCAAAAAGCTCTTTGATACCCTCTCCTACTCGAGTAGGAG AGGGTATCAAAGAGC

Line-1 retroelements. E13.5 or E15.5 embryos were homogenized into single-cell suspensions and cytosolic lysates obtained using a cytosolic extraction buffer as previously described (63). In brief, PBS -washed cell pellets were lysed in 10 mM Hepes, pH 7.9, 10 mM KCl, 1.5 mM MgCl2, 0.34 M sucrose, 10% glycerol, and 0.1% Triton X-100 for 5 min on ice. Cell lysates were treated with Proteinase K at 55°C for 1 hr and with RNase I (Life Technologies) before phenol/chloroform extraction and ethanol precipitation overnight. Isolated DNA was re-suspended in nuclease free H2O and directly subjected to quantitative PCR analysis.

Statistical methods. Data are presented as the mean ± SEM .Prism 6 (GraphPad) was used for statistical analysis. Statistical tests performed are indicated in figure legends. *, $P < 0.05$; **, $P < 0.01$; ***, $P < 0.001$; and ****, $P < 0.0001$.

Results

G37S homozygous mice are perinatal lethal and G37S embryos show increased expression in IFN-stimulated genes

In collaboration with the Dr. Robert Crouch lab of the NIH, we generated *Rnaseh2a-G37S* knock-in mice to mimic the exact mutation present in AGS patients. *Rnaseh2a*$^{G37S/+}$ mice were viable with no evident deleterious phenotype. Breeding of *Rnaseh2a*$^{G37S/+}$ mice generate still-born pups that were homozygotes for the mutation. No viable G37S homozygotes were observed (die within hours after birth). The G37S homozygote embryos were developmentally retarded from an early embryogenesis period of E10.5, present at expected Mendelian ratio, and were approximately 20% smaller in size compared to their uterine mates (data not shown). I also did not observe any inflammation in histology staining of *Rnaseh2a*$^{G37S/G37S}$ embryos including the brain (data not shown). The lack of neuroinflammation could be due to early death of the animal, or due to different disease presentation in mouse versus human. Other AGS mouse models such as *Trex1*-/- or *Samhd1*-/- also lack evidence of neuroinflammation (64, 97).

I next examined whether there is a molecular signature of immune activation in *Rnaseh2a*$^{G37S/G37S}$ embryos, as it would be expected from its association with AGS. I performed RNA-seq analysis comparing gene expression profiles of WT, *Rnaseh2a*$^{G37S/+}$ and *Rnaseh2a*$^{G37S/G37S}$ primary MEFs isolated from E13.5 embryos. I found that 388 genes were

upregulated 2-fold or more in *Rnaseh2a*$^{G37S/G37S}$ MEFs compared to WT; of those, the most enriched gene network was 'immune response' (DAVID GO term analysis, Figure 2.1A, 2.2B). Many of the highly up-regulated genes in *Rnaseh2a*$^{G37S/G37S}$ cells were interferon-stimulated genes (ISGs), such as *Ifit44, Usp18, Ifit1, Rsad2, Isg15, Irf7, and Cxcl10* (Figure 2.1C). I validated increased expression of *Ifit1, Ifit3, Rsad2,* and *Cxcl10* by qRT-PCR (Figure 2.1D). As ISGs provide defense mechanisms against viral infection, I infected WT, *Rnaseh2a*$^{G37S/+}$ and *Rnaseh2a*$^{G37S/G37S}$ primary MEFs with Vesicular stomatitis virus, VSV-PeGFP, to assess their functionality. I found that *Rnaseh2a*$^{G37S/G37S}$ MEFs were highly refractory to VSV infection, as measured by reduced GFP fluorescence at 24 h or by reduced VSV G and M RNA from 6 to 24 h post infection (Figure 2.1E, 2.2F). Taken together, this data showed that the homozygous G37S mutation in mice invokes innate immune activation of ISGs similar to that of AGS patients (60).

Immune activation in *Rnaseh2a*$^{G37S/G37S}$ primary MEFs requires the cGAS-STING innate immune pathway

I next aimed to determine the signaling pathway(s) responsible for the innate immune activation in *Rnaseh2a*$^{G37S/G37S}$ cells. Many of the upregulated ISGs we observed are direct targets of the transcription factor IRF3 (98, 99), which is activated by phosphorylation by TBK1. I treated *Rnaseh2a*$^{G37S/G37S}$ cells with a TBK1 inhibitor BX795, and observed reduced expression of activated genes, *Cxcl10, Ifit1* and *Rsad2* in *Rnaseh2a*$^{G37S/G37S}$ cells (Figure 2.2A), suggesting the involvement of a cytosolic immune sensing pathway. Using short-hairpin RNA directed against *Mavs* or *Sting* (adaptor proteins for cytosolic RNA- or DNA-sensing, respectively) in *Rnaseh2a*$^{G37S/G37S}$ cells, I found that shRNA against *Sting* restored the low expression levels of

Cxcl10 mRNA to WT levels. In contrast, *Mavs*-knockdown significantly reduced poly(I:C)-induced IFN response, but had no effect on the *G37S*-induced ISG expression (Figure 2.2B, 2.2C), suggesting that the G37S mutation leads to activation of a DNA- but not RNA-sensing pathway.

I next used shRNA to knockdown components of the cytosolic DNA-sensing pathway in *Rnaseh2a*$^{G37S/G37S}$ cells and examined expression of ISGs. shSting and shTbk1 effectively restored mRNA levels to those seen in WT cells (Figure 2.2D). A prominent driver of cytosolic DNA detection, cGAS, responds to microbial- or self-DNA and long, homopolymeric RNA/DNA hybrids (64-67, 100). shRNA-mediated knockdown of cGAS in *Rnaseh2a*$^{G37S/G37S}$ cells also returned ISG expression to low WT levels (Figure 2.2D). As the production of cGAMP by cGAS leads to activation of STING-mediated signaling, I next examined the presence of cGAMP in *Rnaseh2a*$^{G37S/G37S}$ cells using the gap-junction transfer cGAMP bioassay (Ablasser et al., 2013). cGAMP can be transferred from producing cells to neighboring cells through gap junctions, thereby enabling a co-culture-based trans-activation assay for cGAMP detection (Ablasser et al., 2013). I co-cultured *Rnaseh2a*$^{G37S/G37S}$ MEFs (producing cells) with human fibroblasts (target cells), and then utilized human-specific primers to probe the immune activation status of the human cells. *Rnaseh2a*$^{G37S/G37S}$ MEFs induced strong immune activation of the human ISGs tested while WT MEFs had no effect (Figure 2.2E). Importantly, I also found that inhibiting gap junctions with carbenoxolone (CBX), a non-toxic gap junction inhibitor, (Figure 2.2D), or trans-well separation, completely abolished *Rnaseh2a*$^{G37S/G37S}$ MEF's trans-activation activity (Figure 2.2E). These data suggest that *Rnaseh2a*$^{G37S/G37S}$ primary MEFs produce cGAMP that activates the STING pathway.

Sting$^{-/-}$ partially rescues perinatal lethality of G37S mice

In the AGS mouse model of *Trex1* gene deletion, viability of *Trex1*$^{-/-}$ mice is extended dramatically when the response to secreted type I IFN is ablated by deleting the interferon-receptor, *Infra1*or by eliminating the adaptive immune response through *Rag2* gene deletion (68). I thus bred G37S to *Infαr1*$^{-/-}$ or *Rag2*$^{-/-}$ backgrounds and found that neither of these genetic knockouts was able to rescue the perinatal lethal phenotype (Table 6). These findings are consistent with lack of inflammation in the *Rnaseh2a*$^{G37S/G37S}$ embryos, further suggesting cell-intrinsic defects may be responsible. Partial rescue of the embryonic development defect seen in *Rnaseh2b*-null mice was obtained by deleting the *p53*$^{-/-}$ gene (87). However, in collaboration with the Dr. Robert Crouch lab of the NIH, we found *Rnaseh2a*$^{G37S/G37S}$ *p53*$^{-/-}$ mice also exhibited perinatal lethality indistinguishable from *Rnaseh2a*$^{G37S/G37S}$ alone. I also did not observe elevated expression of p53 pathway genes from our RNA-seq analysis (data not shown).

I next bred *Rnaseh2a*$^{G37S/G37S}$ onto *Mavs*$^{-/-}$ or *Sting*$^{-/-}$ background. *Rnaseh2a*$^{G37S/G37S}$ remains perinatal lethal on *Mavs*$^{-/-}$ background (Table 6), consistent with RNA-sensing pathways being uninvolved (Figure 2.2). Remarkably, I obtained viable pups of *Rnaseh2a*$^{G37S/G37S}$*Sting*$^{-/-}$ genotype, albeit at 6% of expected frequency (or 2% of weaned pups from heterozygous crosses on the *Sting*$^{-/-}$ background, Table 6). Most of the *Rnaseh2a*$^{G37S/G37S}$*Sting*$^{-/-}$ still exhibited perinatal lethality, similar to *Rnaseh2a*$^{G37S/G37S}$ alone (Table 6), and I did not observe any intermediate phenotypes. I compared ISG expression in primary E14.5 MEFs, and found that *Rnaseh2a*$^{G37S/G37S}$*Sting*$^{-/-}$ completely returned ISG expression to the low level in *Rnaseh2a*$^{+/+}$*Sting*$^{-/-}$, whereas *Mavs*$^{-/-}$ had no effect (Figure 2.3A). I also bred *Rnaseh2a*$^{G37S/G37S}$

onto *cGAS*$^{-/-}$ background and *Rnaseh2a*$^{G37S/G37S}$*cGAS*$^{-/-}$ embryos also restored ISG expression to WT levels (Figure 2.3A). Moreover, the mean ISG score is highly elevated in *Rnaseh2a*$^{G37S/G37S}$ and *Rnaseh2a*$^{G37S/G37S}$*Mavs*$^{-/-}$ MEFs, whereas both *Rnaseh2a*$^{G37S/G37S}$*Sting*$^{-/-}$ and *Rnaseh2a*$^{G37S/G37S}$*cGAS*$^{-/-}$ MEFs show similar baseline values as in WT (Figure 2.3B). I also measured cGAMP in both rescued MEFs using the gap-junction bioassay. Both *Rnaseh2a*$^{G37S/G37S}$ and *Rnaseh2a*$^{G37S/G37S}$*Sting*$^{-/-}$ produce cGAMP as these cellular genotypes have cGAMP-producing cGAS. Deletion of *Cgas* in *Rnaseh2a*$^{G37S/G37S}$*cGAS*$^{-/-}$ MEFs failed to induce transfer of gap-junction based immunity, indicating dependence on the DNA sensor cGAS (Figure 2.3C). These data further demonstrate that the cGAS-cGAMP-STING pathway is mediating the immune activation in G37S mice. Since only a small fraction of the progeny with *Rnaseh2a*$^{G37S/G37S}$*Sting*$^{-/-}$ genotype is viable, our data also suggest that innate immune activation through the cGAS-cGAMP-STING pathway only partially contributed to the lethality of G37S mice.

Table 6: Genetic crosses of G37S mice

Mice	*p53*$^{-/-}$		*INFAR*$^{-/-}$		*Rag2*$^{-/-}$		*Mavs*$^{-/-}$		*Sting*$^{-/-}$	
	Neonates (no. embryos)	Weaned pups (no. mice)	Neonates (no. embryos)	Weaned pups (no. mice)	Neonates (no. embryos)	Weaned pups (no. mice)	Neonates (no. embryos)	Weaned pups (no. mice)	Neonates (no. embryos)	Weaned pups (no. mice)
WT	23% (7)	33% (17)	24% (8)	44% (67)	26% (10)	32% (30)	22% (4)	41% (52)	23% (7)	32% (95)
G37S/+	58% (18)	67% (34)	52% (17)	56% (87)	53% (20)	68% (65)	56% (10)	59% (74)	60% (18)	66% (196)
G37S/ G37S	19% (6)	0% (0)	24% (8)	0% (0)	21% (8)	0% (0)	22% (4)	0% (0)	17% (5)	2% (6)

White-spotting phenotype and increased LINE-1 expression

I also observed several interesting phenotypes in the viable *Rnaseh2a*$^{G37S/G37S}$*Sting*$^{-/-}$ mice. These mice are approximately 70% in body size and weight compared to WT or heterozygous controls (Figure 2.3D). I have observed both male and female progeny for *Rnaseh2a*$^{G37S/G37S}$*Sting*$^{-/-}$, and all have so far failed to produce offspring, whereas littermate controls are fertile. These rescued *Rnaseh2a*$^{G37S/G37S}$*Sting*$^{-/-}$ mice are grossly healthy, with the

oldest animal approaching one year of age. Histopathology analysis did not find any abnormalities or inflammation in internal organs including the brain of *Rnaseh2a*$^{G37S/G37S}$*Sting*$^{-/-}$ mice (data not shown). Collectively, these results suggest an underlying developmental defect in the rescued mice which occurs independently of the cGAS-STING dependent immune sensing observed in *Rnaseh2a*$^{G37S/G37S}$ mice alone.

Intriguingly, all of the viable *Rnaseh2a*$^{G37S/G37S}$*Sting*$^{-/-}$ mice presented a ventral white spotting phenotype, as well as white hind- and fore-paws that are not observed in wild type or heterozygous littermates (Figure 2.3E). This phenotype was consistent from birth and remained throughout the lifespan of the mice. Skin histology from the white patches of *Rnaseh2a*$^{G37S/G37S}$*Sting*$^{-/-}$ mice is structurally normal, although lack of melanin in hair shafts is evident (data not shown). It has been observed mice expressing a conditional, synthetic LINE-1 retroelement present a similar white patching phenotype. Retroelements are ancient viral remnants which have stably integrated into the genome (68). These genetic elements can regulate multiple cellular processes through their genetic replication and insertion into different sites in the genome. LINE-1 retrotransposition was observed to disrupt melanocyte development at an early embryonic time point (130). My observations align with previous literature implicating the dysregulation of endogenous retroelements in the pathogenesis of AGS (68, 101), and it has been proposed that the RNA/DNA hybrids or dsDNA derived from the endogenous retroelement replication cycle can function as ligands of the cGAS-STING pathway (100). I thus measured LINE-1 retroelement in WT, *Rnaseh2a*$^{G37S/G37S}$ and *Rnaseh2a*$^{G37S/G37S}$*Sting*$^{-/-}$ E13.5 and E15.5 embryos. Indeed, I found that LINE-1 DNA level from cytosolic extracts is increased in both *Rnaseh2a*$^{G37S/G37S}$ and *Rnaseh2a*$^{G37S/G37S}$*Sting*$^{-/-}$ embryos to similar levels compared to littermate

WT embryos, suggesting that it is independent of immune activation (Figure 2.3F). It remains unclear whether the increase in LINE-1 DNA is because of an increase in LINE-1 element activity, or because of defects in genomic structures where LINE-1 elements are enriched as was recently suggested (102). Regardless of this distinction, the G37S mutation causes white spotting phenotype in *Rnaseh2a*$^{G37S/G37S}$*Sting*$^{-/-}$ mice, likely resulting from defects in melanocyte's development. G37S mutation also causes increased level of LINE-1 DNA, which may contribute to the activation of the cGAS-STING pathway.

Discussion

In summary, the G37S mouse represents the first RNase H2 mouse model with a clear immune activation phenotype, making it useful for understanding the associated human disease. Embryonic development until birth allowed the expression of innate immune signaling proteins or immune ligands, which uncovered the active cGAS-STING innate immune pathway in G37S mice.

Utilizing a different RNase H2 AGS-mutant mouse model or in RNase H2-deficient cell-line models, other groups have reported similar observations to my work, in that RNase H2 deficiency instigates cGAS-STING immune signaling (119, 120). These reports implicate genotoxicity, which arises in the absence of RNase H2 (87, 88), to activate the cGAS-STING pathway. DNA damage causes fragmentation of the nucleus into structures termed micronuclei which have been proposed to serve as pools of dsDNA for cGAS-dependent recognition (119). This DNA-damage mediated model suggests non-specificity of micronuclei-derived dsDNA as a source of cGAS ligands. I reported an elevation in cytosolic DNA derived specifically from LINE-1 retroelements in the cytosol of G37S cells, suggesting a specificity of certain DNA

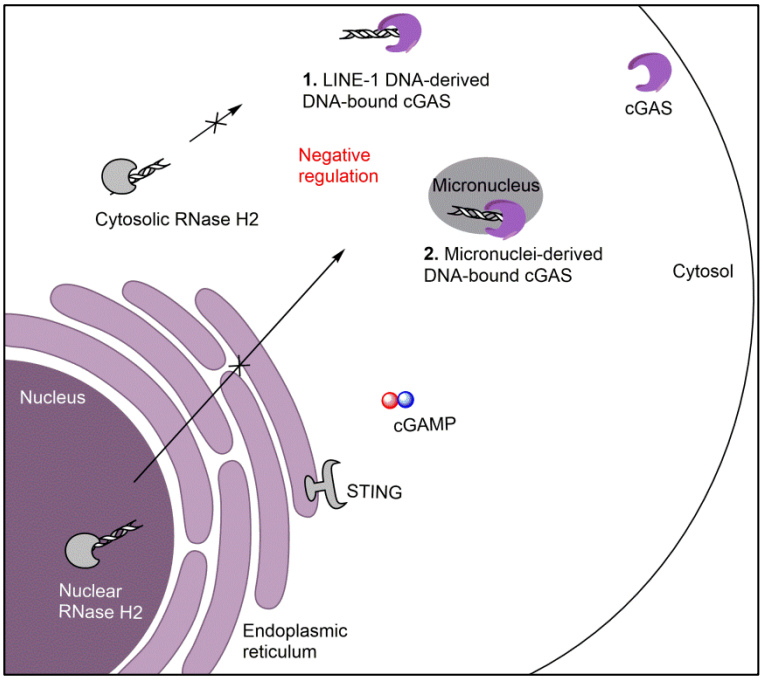

Figure 2.4: RNase H2-mediated regulation of the cGAS-STING pathway

A model of how the cGAS-dependent immune response is restrained by RNase H2.

RNase H2 acts as negative regulator of cGAS activation through the degradation of immunogenic DNA species in the cytosol. The exact source of these species is not well characterized; however, it may derive from RNase H2-mediated degradation of **1. LINE-1 retroelements** or **2. Micronuclei-derived DNA.** Sensing of either type of DNA ligand will instigate cGAS activation, leading to AGS development.

ligands to trigger cGAS-STING signaling during *Rnaseh2*-deficiency. A more comprehensive analysis of cytosolic DNA species was not explored by me and it remains unresolved whether this elevation in cytosolic LINE-1 DNA is simply derived from the pool of micronuclei DNA in G37S cells, or whether RNase H2 specifically regulates LINE-1 retrotransposition events. Direct evidence for the latter RNase H2-dependent retrotransposition model has been published by several independent studies after publication of my work (131, 132); however, more comprehensive experiments aimed at reconciling differences between these two models in the context of AGS must be undertaken in future studies.

The lingering question regarding the source of cGAS ligands during RNase H2 deficiency also invokes another enigma regarding RNase H2 biology, in that which function of the protein is responsible for immune activation in mammalian cells? The G37S mutation will lead to the loss of both of RNase H2's functions: the cleavage of single ribonucleotides within a dsDNA duplex, and the degradation of the RNA strand in RNA: DNA hybrids (94). Either the

accumulation of RNA/DNA hybrids or the accumulation of rNMPs in DNA could instigate genotoxicity within cells, as ribonucleotides are prone to spontaneous hydrolysis and may lead to double-stranded DNA breaks (87, 88). To distinguish between the two activities, a separate mouse model should be established, one that is defective in one activity of RNase H2 but does not impact the other role. In this model, lethality should be observed for, and importantly the investigation of cell-intrinsic immunity should be characterized. Such a mutation has been established in *S. cerevisiae* to unlink the two activities in their contribution to genotoxicity (94); however, this distinction between activities has remained unanswered in higher order organisms. Further biochemical analysis comparing G37S and other existing *Rnaseh2* knockout mouse models are necessary to elucidate the differences in biochemical defects and to shed light on the possible source of nucleic acids that trigger the cGAS-STING pathway in the G37S mice.

The perinatal lethality of the G37S mice is likely caused in large part by a yet-to-be identified biochemical defect associated with the mutation, one that has remained enigmatic. *Tmem173*$^{-/-}$ only partially rescued the lethality, despite complete suppression of ISG expression, and *p53*$^{-/-}$ failed to rescue the lethality. Similarly, another AGS mouse model, the *Adar1*$^{-/-}$ mouse, exhibits early embryonic lethality, and it can be partially by *Mavs*$^{-/-}$ or *Ifih1*$^{-/-}$ (78, 80). These findings indicate that *Rnaseh2* and *Adar1* genes associated with AGS have important functions that are critical for embryonic development in mice, beyond that of prohibiting formation of aberrant nucleic acids that activate innate immunity (78, 82). While the loss of ISGs coincides with the rescued G37S animal on the *STING*$^{-/-}$ background, it may also be possible STING regulates other aspects within cell biology which would explain the partial rescue. Such roles are the subject of intense investigation as STING is an evolutionary conserved protein

predating the type I IFN response in lower order organisms (32). I speculate one role of STING may be related to autophagy regulation within the cell, as this concept has been proposed within this field (32). A potential for enhanced autophagy in the absence of STING may clear damaging micronuclei or genomic debris which could limit embryonic cellular development in G37S mice. It is also possible that loss of STING may positively affect cell-cycle progression as it has been reported *Sting*$^{-/-}$ cells are more resistant to cellular senescence than WT cells (125, 126). In such a scenario, the absence of STING would allow for cells to avoid senescence caused by STING-dependent sensing of micronuclei in the developing G37S mice. Rescued mice would indicate the small fraction that could progress through the cell-cycle rather than undergo cell-cycle arrest as has been reported to occur in the *Rnaseh2b*$^{-/-}$ mouse model (87, 88). As the rescued *Rnaseh2a*$^{G37S/G37S}$*Sting*$^{-/-}$ are born at a very low frequency, it is experimentally challenging to track and define early stage embryos which can overcome these defects in development. Regardless of the unresolved questions in RNase H2-mutant mediated AGS, our genetic and immunological analysis of the G37S mice establish a critical role of the cGAS-STING pathway in AGS, and suggest that therapeutic intervention of this pathway may be beneficial for treating patients diagnosed with this subtype of the disease.

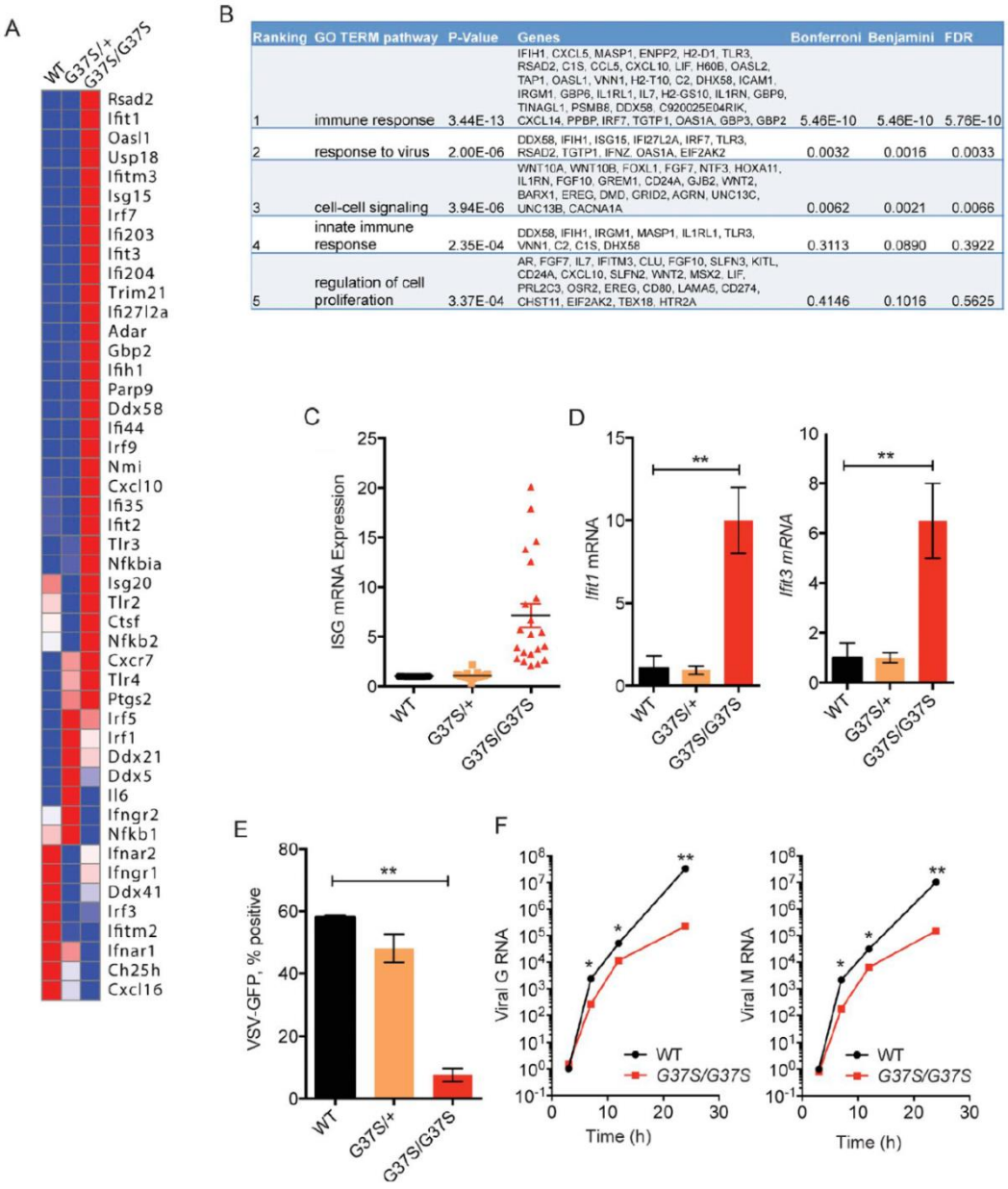

Figure 2.1: Primary cells from *Rnaseh2a*$^{G37S/G37S}$ embryos show increased expression in ISGs.
(A) A heat map of immune gene expression in WT, *Rnaseh2a*$^{G37S/+}$ and *Rnaseh2a*$^{G37S/G37S}$ primary MEF s. Data from RNA -seq. **(B)** Gene ontology analysis of 388 genes that are increased by twofold or more in *Rnaseh2a*$^{G37S/G37S}$ compared with WT MEF s. Top five enriched pathways are shown. **(C)** Expression of ISG s in WT, *Rnaseh2a*$^{G37S/+}$, and *Rnaseh2a*$^{G37S/G37S}$ primary MEFs. Each dot represents a different ISG. Data from RNA -seq. **(D)** Quantitative RT-PCR analysis of *Ifit1* and *Ifit3* mRNA (ISG s) in WT, *Rnaseh2a*$^{G37S/+}$, and *Rnaseh2a*$^{G37S/G37S}$ primary MEFs. **(E)** VSV -GFP replication in WT, *Rnaseh2a*$^{G37S/+}$, and *Rnaseh2a*$^{G37S/G37S}$ primary MEFs. FACS analysis measures VSV-GFP signal at 24 h after infection. Quantitative RT-PCR analysis of VSV G and M RNA measure viral RNA replication at indicated time after infection **(H)**. *, $P < 0.05$; **, $P < 0.01$. Mice were compared with littermate controls. Data are representative of at least three independent experiments. Error bars represent the SEM . Unpaired Student's t test (C–F).

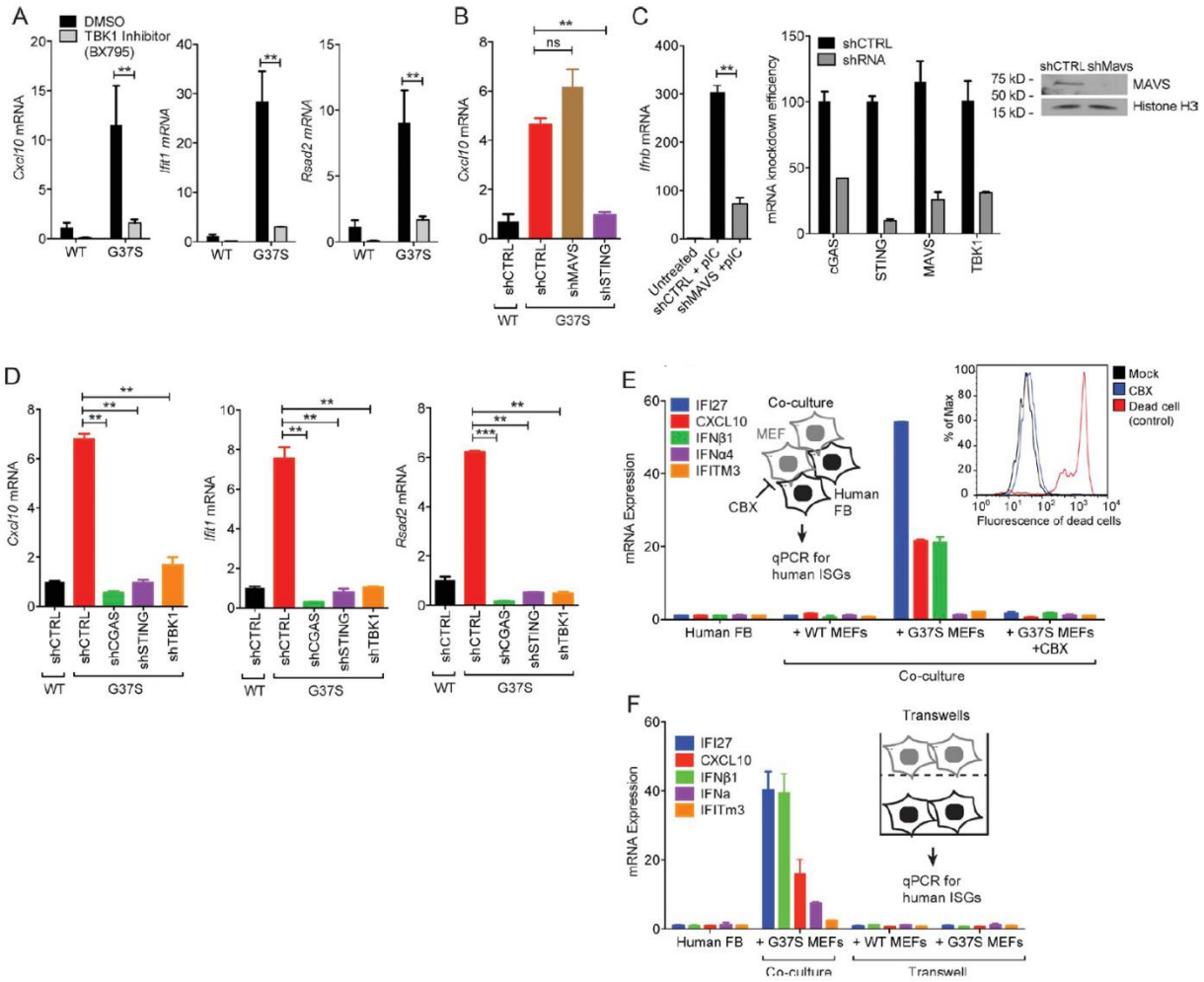

Figure 2.2: Immune activation in *Rnaseh2a*$^{G37S/G37S}$ primary MEFs requires the cGAS–STING innate immune pathway. (A) Quantitative RT-PCR analysis of *Cxcl10*, *Ifit1* and *Rsad2* mRNA (all ISG s) in WT and *Rnaseh2a*$^{G37S/G37S}$ (G37S, same below) MEF s treated with DMSO or TBK1 inhibitor BX795 (10 μM) for 6 h. **(B)** Quantitative RT-PCR analysis of *Cxcl10* mRNA in WT and G37S MEF s treated with shRNA against indicated genes involved in cytosolic nucleic acid-sensing. **(C)** shMAVS knockdown reduces poly(I:C)-induced IFN response. Knockdown efficiency is shown on the right. **(D)** Quantitative RT-PCR analysis of *Cxcl10*, *Ifit1*, and *Rsad2* mRNA in WT and G37S MEF s treated with shRNA against indicated genes involved in DNA -sensing pathway. **(E)** Quantitative RT-PCR analysis of a panel of human ISG s and IFN genes in human fibroblasts (BJ-1 cells) co-cultured with WT or G37S MEF s for 18 h, with or without CBX treatment (inhibits gap junction). Left inset shows a schematic diagram of the gap junction assay. Right inset shows FAC S analysis of cell death in mock- and CBX -treated cells. **(F)** Quantitative RT-PCR analysis of human ISG s in human fibroblasts in a trans-well assay co-cultured with WT or G37S MEFs for 18 h. Mice were compared with littermate controls. **, $P < 0.01$; ***, $P < 0.001$. ns, not significant. Data are representative of at least three independent experiments. Error bars represent the SEM . Unpaired Student's t test (A–D).

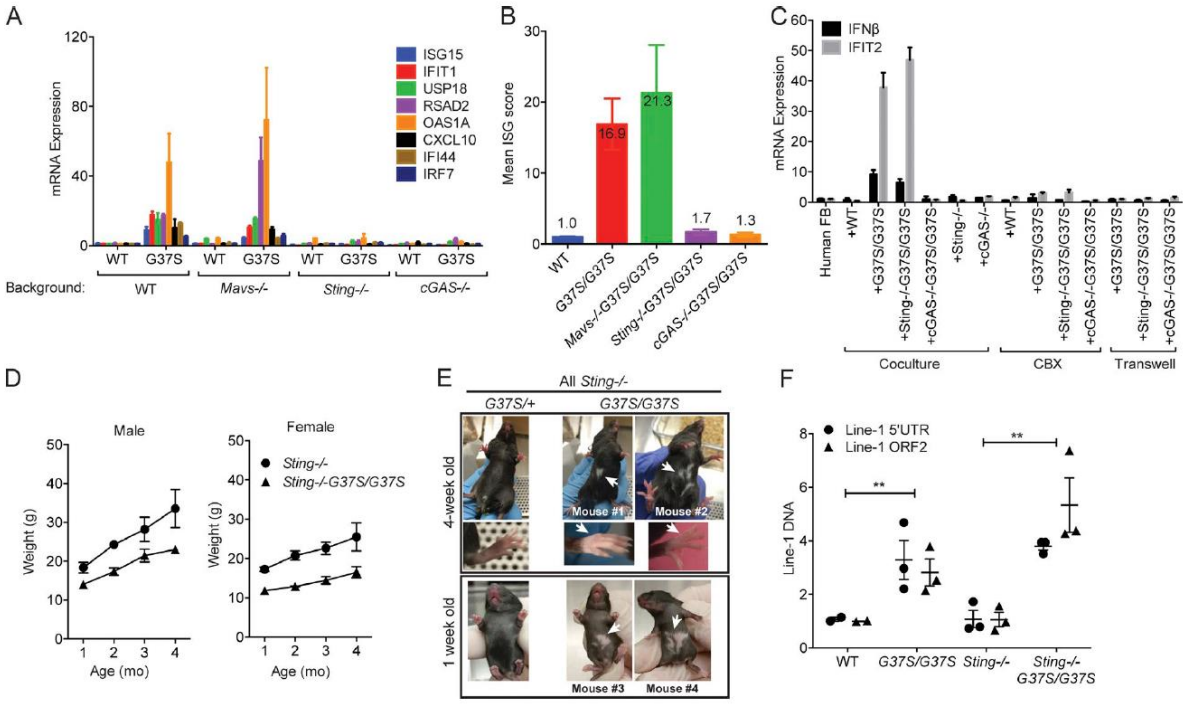

Figure 2.3: *Sting*$^{-/-}$ partially rescues perinatal lethality of G37S mice. (A) Quantitative RT-PCR analysis of a panel of mouse ISGs in WT or G37S embryos on *Mavs*$^{-/-}$ or *Sting*$^{-/-}$ or *Cgas*$^{-/-}$ background. Total RNA was isolated from primary MEFs (E13.5) of indicated genotype. **(B)** Mean ISG score of indicated genotypes. Data from A. **(C)** Gap junction cGAMP bioassay. As in Fig. 2E, MEFs of indicated genotype were co-cultured with human BJ-1 cells for 18 h, with or without CBX or direct contact (indicated on the bottom). Quantitative RT-PCR analysis of *IFNβ* and *IFIT1* indicates cGAMP activity in MEF s. **(D)** Mouse body weights. n = 4. **(E)** White-spotting phenotype in *Rnaseh2a*$^{G37S/G37S}$ *Sting*$^{-/-}$ viable adults. **(F)** Quantitative PCR analysis of mouse Line-1 5′ UTR and ORF2 DNA in WT or G37S embryos (isolated from E13.5 or E15.5; n = 3). Each dot represents an individual embryo. Mice were compared with littermate controls and with age-matched knock-out mice **, $P < 0.01$. Data are representative of at least two independent experiments (A–C), or pooled data from multiple animals (D–F). Error bars represent the SEM. Unpaired Student's t test (F).

CHAPTER THREE

TOLLIP PREVENTS IRE1α-MEDIATED STING DEGRADATION AT THE RESTING STATE TO ESTABLISH IMMUNE HOMEOSTASIS

Introduction

The innate immune system senses non-self or altered-self molecular structures through pattern recognition receptors in order to eliminate pathogens or damaged cells, and restore an organism to its basal physiology. One important innate immune signaling pathway responsible for detecting several microbial and viral pathogens is the cGAS-STING pathway (27-30). The cytosolic localization of the innate immune sensor cGAS gives the sensor an indispensable role in detecting double-stranded DNA of non-self or self-origin (21, 22). After binding to DNA, cGAS produces a cyclic-dinucleotide, 2'3'-cGAMP, which activates STING, an ER-localized protein (25). STING activation induces its translocation to ER-Golgi-intermediate compartments (ERGIC) where it aggregates and activates branching TBK1-IRF3 and NF-κB axes, transcription factors required for the induction of type I interferon, and inflammatory cytokines, respectively (32). Following activation, STING embarks on a trafficking route from the ER to aggregated vesicles where it activates downstream signaling and is then degraded through lysosome-mediated autophagy (35). Such a degradative mechanism resembles the final signaling cascade of the TLR4 receptor, where after receptor ligation and internalization, TLR4-containing endosomes fuse with lysosomes for cessation of sensing (103).

While activation-induced lysosomal degradation of STING is acknowledged, studies addressing the mechanism that maintains resting state STING protein levels have largely focused on proteasome-mediated degradation (46, 49-54). A fraction of STING is channeled towards degradation through a proteosomal pathway initiated by addition of K48-ubiquitin chains. This proteosomal degradation is antagonized by iRHOM2 and the deubiquitinase EIF3S, thereby allowing optimal STING signaling to occur (49). iRHOM2 has been previously reported to influence TLR-mediated responses as well (129). Whether STING can be targeted by degradation through other means and how resting-state STING protein level is maintained are unclear and vital to understand. Chronic STING activation can lead to the development of fatal auto-inflammatory and autoimmune diseases (64, 104). Reduced STING protein level has also been found in several cancers (105, 106). As STING plays a critical role in infection, autoimmune disease and cancer, a better understanding of the mechanism of basal STING regulation will have broad clinical implications.

In this study, I discovered TOLL interaction protein (TOLLIP) as a critical regulator of STING. TOLLIP regulates resting-state STING protein levels as well as downstream immune signaling in a process dependent on the ER protein IRE1α and lysosomes. I also found that *Tollip*-deficiency occludes development of STING-mediated auto-inflammatory disease in *Trex1*$^{-/-}$ mice.

Experimental Procedure

Mice, cells, and viruses. *Tollip*$^{-/-}$ mice were obtained from Dr. Michel Maillard (CHUV) Primary MEFs were isolated from embryos of either E10 or E13.5 embryonic dates. These cells

were maintained in DMEM with 10% (vol/vol) heat-inactivated FCS, 2 mM l-glutamine, 10 mM Hepes, and 1 mM sodium pyruvate (complete DMEM) with the addition of 100 U/ml penicillin and 100 mg/ml streptomycin and were cultured at 37°C with 5% CO2. Experiments performed in BSL-2 conditions were approved by the Environmental Health and Safety Committee at University of Texas Southwestern Medical Center. Experiments involving mouse materials were approved by the Institutional Animal Care and Use Committees of the University of Texas Southwestern Medical Center.

Reagents and antibodies

Herring testis DNA was used as dsDNA for immune stimulations (Sigma). 2'3'-cGAMP and DMXAA were used for STING agonists (Invivogen). PolyI:C was transfected as a MAVS-pathway agonist (Invivogen). Lipofectamine 2000 was used as transfection reagent for intracellular stimulations (Thermo Fisher).

Antibodies: ATF4 (CST D4B8), ATF6 (CST D4Z8V), BIP (CST C50B12), CHOP (CST L63F7), phospho-EIF2α (CST D968), HMGB1 (Abcam 18256), IRAK1 (CST D5167), IRE1α (CST 14C10), phospho-IRE1α (Thermo Fisher PA1-16927), IRF3 (CST D83B9), phospho-IRF3 (CST 4D4G), MAVS (CST 4983), STING (CST D2P2F), TOLLIP (Abcam ab187198), goat anti-rabbit IgG (Biorad 1706515), goat anti-mouse IgG (Biorad 1706516).

Western blotting

Cells were lysed in RIPA buffer (150mM NaCl, 5mM EDTA, 50mM Tris, 1.0% NP-40, 0.5% sodium deoxycholate, 0.1% SDS) supplemented with protease and phosphatase inhibitors then

centrifuged at 4°C to obtain cellular lysate. Equal amounts of protein (10-50μg) were loaded into a 12% SDS-PAGE gel. Semi-dry transfer onto nitrocellulose membrane was performed. Membrane was blocked in 5% milk in TBS-T buffer for one hour at room temperature, followed by overnight incubation in 3% milk in TBS-T with primary antibodies. Membrane was washed with TBS-T buffer, incubated at room temperature with HRP-conjugated IgG secondary antibody, washed with TBS-T, and then developed with SuperSignal West Pico Chemiluminescent Substrate (Thermo Fisher) or SuperSignal West Femto Maximum Sensitivity Chemiluminescent Substrate (Thermo Fisher).

Compound inhibition

Protein degradation inhibition: Cells were seeded overnight, then treated with 5mM 3-MA (Invivogen tlrl-3ma), 0.5μM Bafilomycin A1 (Invivogen tlrl-baf1), and 5μM MG-132 (Sigma 133407-82-6) for 16 hours. Cells were then collected and lysed in RIPA buffer for Western blot analysis.

IRE1α inhibition: Cells were seeded overnight, and then treated with 100μM 4μ8C (Sigma SML0949) for 24 hours. Cells were then collected and lysed in RIPA buffer for Western blot analysis.

siRNA knockdown Pre-designed siRNA oligomers were obtained from Sigma-Aldrich and re-suspended in water at 20μM. 10^5 MEFs were plated and transfected with siRNA in Optimem media (Thermo Fisher) for 48 hours with lipofectamine RNAiMAX (Thermo Fisher) then

validated for knockdown efficiency with RT-PCR or Western blotting. Oligos with efficient knockdowns (>50% mRNA reduction) were used in subsequent experiments.

Table 7: siRNA oligos

Oligo	**Sequence (5'-3')**
Tollip #1 s	CCAUCAAUCCUUGCUGCA
Tollip #1 as	UGCAGCAAGGAAUUGAUGG
Tollip #2 s	GCACUUACUUACAGGUUAU
Tollip #2 as	AUAACCUGUAAGUAAGUGC
Tollip #3 s	GAGUUCAUGUGCACUUACU
Tollip #3 as	AGUAAGUGCACAUGAACUC
Tollip #4 s	CCAAGAACCCUCGCUGGAA
Tollip #4 as	UUCCAGCGAGGGUUCUUGG

LentiCRISPR CRISPR oligos against *Tollip (*Fwd 5'-3': CACCGCCCTTACTGCCGTCTGCGTC; Rev primer 5'-3': AAACGACGCAGACGGCAGTAAGGGc) were designed for the LentiCRISPRv2 plasmid (Feng Zhang, Broad Institute). Oligos were cloned into the plasmid according to recommended instructions (GeckoCRISPRv2). Final plasmid was transfected into Lenti-X 293T cells along with lentiviral packaging plasmids psPAX2 and pMD2.G. Cell culture media was collected 72 hours after transfection and concentrated with Lenti-X concentrator overnight, then re-suspended in 1/10 of original supernatant in DMEM media. CRISPR-harboring lentiviruses were allowed to infect cells overnight with polybrene (10μg/ml) treatment, and cells expressing the plasmid were selected with a puromycin concentration (Life Technologies) for several days. Single cell clones were identified by Western blotting for cells lacking protein expression.

RNA isolation and quantitative RT-PCR. Total RNA was isolated with TRI reagent according to the manufacturer's protocol (Sigma-Aldrich), and cDNA was synthesized with iScript cDNA

synthesis kit (Bio-Rad Laboratories). iTaq Universal SYBR Green Supermix (Bio-Rad Laboratories) and an ABI-7500 Fast Real-Time PCR system (Applied Biosystems) were used for quantitative RT-PCR analysis.

Table 8: RT-PCR oligos

Oligo	**Sequence (5'-3')**
Chop Fwd:	TTGCCCTCTTATTGGTCCAGC
Chop Rev:	TAGCGACTGTTCTGTTCCCAC
Cxcl10 Fwd:	GGGATCCCTCTCGCAAGGACGGTCC
Cxcl10 Rev:	ACGCTTTCATTAAATTCTTGATGGT
Ifit2 Fwd:	GGAGAGCAATCTGCGACAG
Ifit2 Rev:	GCTGCCTCATTTAGACCTCTG
Ifit3 Fwd:	TGGCCTACATAAAGCACCTAGATGG
Ifit3 Rev:	CGCAAACTTTTGGCAAACTTGTCT
Ifitm3 Fwd:	CCCCCAAACTACGAAAGAATCA
Ifitm3 Rev:	ACCATCTTCCGATCCCTAGAC
Ifnb Fwd:	CTGCGTTCCTGCTGTGCTTCTCCA
Ifnb Rev:	TTCTCCGTCATCTCCATAGGGATC
Oas1a Fwd:	GCCTGATCCCAGAATCTATGC
Oas1a Rev:	GAGCAACTCTAGGGCGTACTG
Sting Fwd:	TCAGTGGTGCAGGGAGCCGA
Sting Rev:	CGCCTGCTGGCTGTCCGTTC
Tollip Fwd:	CCTCAGCCCCGCTGTAATG
Tollip Rev:	CAGCATCTTTGTTCCCTCTCTG
Usp18 Fwd:	TGCCTCGGAGTGCAGAAGA
Usp18 Rev:	CGTGATCTGGTCCTTAGTCAGG
Xbp1 Fwd:	TGCTGAGTCCGCAGCAGGTG
Xbp1 Rev:	GCTGGCAGGCTCTGGGGAAG
Spliced Xbp1 Fwd:	CGATGGGAAGATGTTCTGGG
Spliced Xbp1 Rev:	ACACGCTTGGGAATGGACAC

Statistical methods. Data are presented as the mean ± SEM .Prism 6 (GraphPad) was used for statistical analysis. Statistical tests performed are indicated in figure legends. *, $P < 0.05$; **, $P < 0.01$; ***, $P < 0.001$; and ****, $P < 0.0001$.

Results

TOLLIP is required for the STING-mediated immune response

Through a pilot genome-wide screening approach, I had identified a candidate list of genes which may play a role in regulating the expression of STING protein (data not shown). The targets from this screen were subjected to a secondary arrayed screening approach using pooled siRNA oligos in order to assess which genetic perturbations could impact the cellular response to 2'3'-cGAMP, but not intracellular dsRNA. I identified TOLLIP as a critical regulator of the STING-mediated IFN response in this arrayed siRNA screen. Pooled siRNA knockdown of *Tollip* in wild type MEFs potently inhibited the intracellular 2'3' cGAMP- but not the dsRNA-induced IFN response (Figure 3.1A, 3.1B). This pooled oligo mixture was then separated into its constituent sequences, and each different oligo was used in a knockdown of *Tollip.* Knockdown cells were then stimulated with cGAMP and *Ifnb* mRNA induction was measured. I observed a dose-dependent requirement of TOLLIP in the cGAMP-induced IFN response, as the levels of TOLLIP mRNA positively correlated with STING-signaling output (Figure 3.1C). The impairment of STING-signaling in *Tollip*-knockdown cells persisted throughout a time-course of stimulation and under a broad-range of cGAMP concentrations (Figure 3.1D, 3.1E). These results demonstrate *Tollip*-deficiency negatively affects the STING response throughout stimulation, rather at a single time point, and that saturating amounts of STING ligand could not induce a similar immune response as WT cells. Downstream of STING are two transcription factor pathways, IRF3 and NF-κB. *Tollip*-knockdown significantly inhibited immune genes by both of the aforementioned pathways by the cell-permeable STING agonist DMXAA, suggesting TOLLIP plays a role either at both branches of the STING

pathway, or at a common step above the bifurcation, potentially at the level of STING (Figure 3.1F). The reduced immune gene expression was restored in *Tollip*-knockdown cells when they were reconstituted with wild type TOLLIP (siRNA-resistant, Figure 3.1G), suggesting that TOLLIP itself, rather than an off-target effect, is required for STING signaling activation. *Tollip*$^{-/-}$ MEFs also showed a reduced response to DMXAA but not to intracellular dsRNA (Figure 3.1H, 3.1I). Bone marrow-derived macrophages (BMDMs) isolated from *Tollip*$^{-/-}$ mice were also dampened in response to cGAS or STING ligands (Figure 3.11J). These results collectively suggest that TOLLIP regulates the STING signaling pathway.

TOLLIP maintains the resting-state STING protein level

Activation of STING induces post-translational modifications of the protein, thereby allowing it to activate the transcription factor IRF3 before STING is subjected towards ligand-induced degradation (35). I analyzed STING signaling kinetics by immunoblots of STING protein and IRF3 phosphorylation. *Tollip*-knockdown cells showed reduced IRF3 phosphorylation after DMXAA stimulation and a similar rate of STING degradation compared to control cells (Figure 3.2A). Importantly, I observed substantially reduced STING protein level in unstimulated *Tollip*-knockdown cells compared to control cells, suggesting that Tollip plays a role in maintaining resting-state STING protein level. *Sting* mRNA levels are the same in control and *Tollip*-knockdown cells, indicating this difference in STING protein was post-transcriptional (Figure 3.2B). I also did not observe any changes in MAVS protein (involved in RNA sensing) or IRAK1 protein (involved TLR signaling) in *Tollip*-knockdown cells compared to control cells indicating specificity for STING (Figure 3.2A). *Tollip*$^{-/-}$ MEFs also contain reduced STING

protein, but not mRNA, as compared to WT MEFs, and stable expression of wild type TOLLIP (using a retroviral vector) in *Tollip*$^{-/-}$ MEFs completely restored STING protein to the WT level (Figure 3.2C, 3.2D) suggesting TOLLIP function to stabilize STING protein at the resting-state.

I next investigated which protein degradation pathways may be responsible for the decreased level of STING protein in *Tollip*$^{-/-}$ cells. I treated *Tollip*$^{-/-}$ cells with inhibitors for autophagosome formation (3-MA), proteosomal degradation (MG-132), and lysosomal acidification (BafA1). I observed that *Tollip*$^{-/-}$ cells treated with BafA1 completely restored STING protein to the wild type level, while MG132 treatment only led to a slight increase (Figure 3.2E). I speculate the partial increase in STING protein caused by MG132 treatment was due to antagonism of basal STING protein degradation through separate and non-related proteosomal degradative pathways previously described (51-54).

It has previously been shown that STING activated by DNA transfection is rapidly degraded through trafficking to the lysosomes (35). I thus examined whether STING may be auto-activated in *Tollip*$^{-/-}$ cells by comparing basal ISG expression in WT and *Tollip*$^{-/-}$ cells. Both genotypes expressed similar levels of ISGs, with no consistent trend in ISG upregulation in the *Tollip*$^{-/-}$ cells (Figure 3.2F). This lack of upregulation is in contrast to what is observed in *Rnaseh2a*$^{G37S/G37S}$ ISGs when compared against those of WT cells (Figure 2.1D). These results suggest TOLLIP prevents resting-state STING protein degradation principally through a lysosomal-mediated degradative pathway independent of STING protein activation.

TOLLIP negatively regulates IRE1α

Lysosomal-mediated degradation of STING protein has recently been reported to coincide with activation of the unfolded protein response (UPR), a pathway that counters endoplasmic reticulum stress (107). ER stress occurs during accumulation of unfolded proteins in the ER. Mammalian cells contain three major UPR effectors, IRE1α, PERK and ATF6 (108). Each UPR effector instigates a distinct regulatory pathway which acts to restore protein folding in the ER. If ER stress is too severe and chronic, these effectors can induce cell death to clear damaged cells within the host (133). To assess activation of the UPR in *Tollip*$^{-/-}$ cells, I measured several UPR-dependent genes that are known to be activated by each of the three major UPR pathways. ATF6- or PERK-dependent genes were not upregulated in *Tollip*$^{-/-}$ cells compared to WT cells (Figure 3.3A). In contrast, *Xbp1* mRNA splicing, a marker for IRE1α activation, was significantly upregulated in *Tollip*$^{-/-}$ cells compared to WT cells (Figure 3.3A). Stable expression of wild type Tollip suppressed *Xbp1* mRNA splicing in *Tollip*$^{-/-}$ cells back to WT levels (Figure 3.3A). These data suggest that *Tollip*-deficiency leads to chronic activation of the IRE1α-mediated UPR pathway.

To further substantiate these findings, I assessed induction of the UPR after treating cells with ER stress-inducing agent thapsigargin (Tg). Compared to WT cells, *Tollip*$^{-/-}$ cells showed an elevation in IRE1α protein at the basal state, an indication of the protein's activation. Furthermore, Tg-induced ER stress led to an increase in BIP protein, an IRE1α-regulated chaperone, to a greater extent in *Tollip*$^{-/-}$ cells compared to WT cells, indicating enhanced signaling through the UPR IRE1α branch (Figure 3.3B). In contrast, other UPR effectors such as CHOP, phospho-eIF2α and ATF4 (downstream of PERK) were induced equally by Tg in WT

and *Tollip*$^{-/-}$ cells (Figure 3.3B). ER stress induces cleavage of ATF6 from a full-length 90-kDa protein (ATF6 p90) to a 50-ka protein (ATF6 p50) (133). Tg-treated and non-treated *Tollip*$^{-/-}$cells displayed reduced ATF6 cleavage compared to WT cells (Figure 3.3B), suggesting these cells have reduced basal activity of the ATF6 branch. I speculate this reduction of the UPR may reflect altered UPR homeostasis caused by active IRE1α activity in the *Tollip*$^{-/-}$ cells. These results collectively demonstrate that *Tollip*-deficiency selectively activates the IRE1α branch of the UPR in the basal state and after induction of ER stress.

IRE1α regulates resting-state STING protein level independently of XBP1

Since *Tollip*-deficiency leads to increased activity of IRE1α and decreased STING protein level, I next assessed whether IRE1α regulates STING's protein level. Interestingly, I found that, at resting-state, STING protein level is substantially higher in *Ire1a*$^{-/-}$ cells compared to WT cells, while *Sting* mRNA levels are similar in both cells (Figure 3.4A, 3.4B). I next examined whether IRE1α is responsible for the reduced STING protein level in *Tollip*$^{-/-}$ cells. I used siRNA to knockdown *Tollip* in WT and *IRE1a*$^{-/-}$ cells. Knocking down *Tollip* in WT MEFs led to reduced STING protein level as expected; however, *Tollip*-knockdown did not alter STING protein level in *IRE1a*$^{-/-}$ cells, suggesting that IRE1α is required for STING protein degradation in cells that lack TOLLIP (Figure 3.4C). I also performed a complimentary experiment where I inhibited IRE1α activity with a small molecule compound 4u8C in WT and *Tollip*$^{-/-}$ cells. Treatment of *Tollip*$^{-/-}$ cells with 4u8C restored STING protein level to that observed in WT cells, further supporting that IRE1α plays an important role in regulating resting-state STING protein level (Figure 3.4D).

When IRE1α is activated, it induces two processes via its RNase domain: the cleavage of *Xbp1* mRNA to its spliced form; and the degradation of cytosolic RNA, a process termed regulated IRE1α-dependent decay (RIDD). To distinguish between these two functions, I assessed XBP1's role in regulating STING protein level by examining WT and *Xbp1*$^{-/-}$ cells. Surprisingly, *Xbp1*$^{-/-}$ cells displayed a lower basal amount of STING protein resembling that of the *Tollip*$^{-/-}$ cells (Figure 3.4E). Several studies have demonstrated that *Xbp1*$^{-/-}$ cells serve as a cellular model for chronically activate IRE1α due to the loss of a regulatory feedback loop limiting IRE1a activation (108-110). Similar to *Tollip*$^{-/-}$ cells, STING in *Xbp1*$^{-/-}$ cells may thus also undergo IRE1α-dependent degradation. To test this hypothesis, I treated *Xbp1*$^{-/-}$ cells with 4u8C to inhibit IRE1α, and indeed I observed restoration of STING protein to the WT level. These data collectively suggest that in two cellular models of chronic IRE1α activation, resting-state STING protein is reduced compared to WT cells and this occurs independently of XBP1, indicative of a role for RIDD in this phenomenon.

Tollip$^{-/-}$ ameliorates STING-mediated autoimmune disease in *Trex1*$^{-/-}$ mice

To examine the in vivo function of TOLLIP in regulating the STING-mediated immune response, I crossed *Tollip*$^{-/-}$ mice to an autoimmune mouse model *Trex1*$^{-/-}$. TREX1 (also known as DNASEIII) is a cytosolic DNase which plays an important role in degrading self-DNA in the cytoplasm. *Trex1*-deficiency leads to accumulation of self-DNA in the cytosol which activates the cGAS-STING pathway and leads to severe systemic autoimmune and auto-inflammatory disease pathology (63, 68). Genetic ablation of either cGAS or STING fully rescues *Trex1*$^{-/-}$ mouse disease (65 67). Since *Tollip*$^{-/-}$ mice are healthy with no detectable immune phenotypes, I

bred the *Trex1*$^{-/-}$ mice on to the *Tollip*$^{-/-}$ background and analyzed disease outcomes of the *Trex1*$^{-/-}$*Tollip*$^{-/-}$ mice.

I found that *Trex1*$^{-/-}$ mice, due to severe auto-inflammatory disease, exhibit decreased body size and weight compared to littermate WT mice (produced by *Trex1*$^{+/-}$ crosses). Remarkably, *Trex1*$^{-/-}$*Tollip*$^{-/-}$ mice are equal in size and weight as WT or *Tollip*$^{-/-}$ mice (Figure 3.5A). *Trex1*$^{-/-}$*Tollip*$^{-/-}$ mice also display no visible signs of health issues such as hunched back, ungroomed fur or body trembling that is often observed in *Trex1*$^{-/-}$ mice (data not shown). I also analyzed tissues of WT, *Trex1*$^{-/-}$, *Tollip*$^{-/-}$ and *Trex1*$^{-/-}$*Tollip*$^{-/-}$ mice. *Trex1*$^{-/-}$ mice develop splenomegaly and inflammation in multiple tissues especially the heart leading to the majority of the animals succumbing to severe myocarditis (64). I found that *Trex1*$^{-/-}$*Tollip*$^{-/-}$ mouse heart lacked signs of inflammatory cell infiltrates and is much improved comparing to *Trex1*$^{-/-}$ mouse heart (Figure 3.5B). *Trex1*$^{-/-}$*Tollip*$^{-/-}$ mouse spleens were also significantly smaller in size compared to *Trex1*$^{-/-}$ mice spleens (Figure 3.5C). BMDMs from *Trex1*$^{-/-}$*Tollip*$^{-/-}$ mice show significantly reduced expression of several ISGs compared to *Trex1*$^{-/-}$ BMDMs (Figure 3.5D), consistent with impaired STING signaling. Together, these data demonstrate that *Tollip*-deficiency impairs STING signaling and ameliorates STING-mediated auto-inflammation in vivo.

Discussion

Through a genetic screen, I identified TOLLIP as a novel regulator of the STING-signaling pathway. Specifically, through regulation of resting-state STING protein level, TOLLIP fine-tunes the cellular response to DNA or cyclic dinucleotides. Mechanistically,

TOLLIP negatively regulates the UPR effector protein IRE1α. *Tollip*-deficiency chronically activates a previously uncharacterized IRE1α-lysosome pathway that selectively degrades STING. This regulation has important implications for auto-inflammatory diseases caused by cGAS-STING, as ablation of *Tollip* in *Trex1*$^{-/-}$ mice ameliorated symptoms of immune disease.

TOLLIP was originally identified as a negative regulator of the TLR2, TLR4 and IL-1R signaling pathways in vitro through overexpression studies (111-112). In vivo characterization of the *Tollip*$^{-/-}$ mouse demonstrated a minor reduction in immune gene induction following TLR or IL-1R signaling pathways (113). The defect in the induced immune response in *Tollip*$^{-/-}$ mice or cells was not in the TLR or IL-1R protein signaling cascades, but was rather at the transcription of inflammatory genes following receptor ligation (113). One interpretation of these results is that the absence of TOLLIP may indirectly impair immune gene induction through separate signaling pathways. An early report on the DNA sensor cGAS implicated the cGAS-STING pathway in regulating the basal expression of immune genes (134). In the absence of cGAS, induction of immune genes was slightly impaired in response to non-DNA PAMPs in a manner dependent on canonical cGAS-STING signaling. An explanation for this phenomenon is that the cGAS-STING pathway normally senses cytosolic dsDNA which passively or actively translocates from the nucleus or the mitochondria during the resting-state. This basal sensing of DNA debris may thus contribute to steady-state expression of immune cytokines. I speculate that the reduction of STING-signaling in *Tollip*-deficient cells may thus also impact this basal priming of immune genes, thereby leading to some reduction of immune signaling for non-cGAS-STING mediated immune pathways originally reported in the first description of the *Tollip*$^{-/-}$ mouse.

My study has demonstrated that in two models of selective and chronic activation of IRE1α, *Tollip*$^{-/-}$ and *Xbp1*$^{-/-}$ cells, STING protein is reduced compared to WT cells in a manner dependent on IRE1α RNase activity. In *Tollip*$^{-/-}$ cells, this reduction in basal STING protein is caused lysosomal-mediated degradation dependent on IRE1α RNase activity but not XBP1. How IRE1α, or its RNase activity in particular, recruits lysosomes to degrade STING remains unclear. The RIDD pathway functions to cleave RNA proximal to IRE1α's ER localization (114). In *D. melanogaster*, RIDD can regulate key biological processes within cells through the degradation of mRNA or regulatory RNA (114). RIDD's role in mammalian cells is relatively unexplored, particularly in the context of innate immunity. Chronic activation of RIDD can cleave miRNA miR-125a which impedes apoptotic programs within cells (108). This miR-125a degradation has implications in antiviral immunity, as cells are rendered more susceptible to viral infections. Chronic RIDD does not impact the innate immune response following RNA virus infection; however, the immune response downstream of DNA viruses was not reported. I hypothesize that RIDD may regulate STING protein through the regulation of ER biology, specifically autophagy of the ER, or through a separate process termed ER-phagy. The degradation of the ER has been implicated in STING protein degradation (107); however, ER-phagy remains incompletely understood in the context of this immune pathway, and as a process itself. Future work should determine the exact RIDD RNA targets which are degraded in *Tollip*$^{-/-}$ cells and which of these targets is responsible for STING protein degradation.

It has been reported that TOLLIP functions as a selective autophagy receptor for proteins harboring polyQ rich domains that are associated with neurodegenerative diseases such as Huntington's disease (HD) (135). Accumulation of neurodegenerative-related protein aggregates

in cells may activate ER stress and the UPR (139). I speculate that in *Tollip*-deficient cells, the accumulation of proteins with polyQ tracts may lead to STING protein degradation through either a selective activation of IRE1α or a weak induction of ER stress below the limits of detection in the assays utilized in this work. In either scenario, the implications of this work suggest broader implications of STING in neurodegenerative disease. If my findings regarding STING are observed in cells derived from HD patients, it is of interest to determine the significance, as loss of STING may influence an aspect of HD development. As HD is associated with inflammation, it is likely this role of STING would be independent of innate immune signaling (136). The understanding of additional roles for STING independent of immune gene induction is a focus of great study as STING predates the evolution of the type I IFN response (32).

The relationship between the IRE1α-mediated stress response and the STING-mediated antiviral response may have broad implications in many disease conditions. It is established that obesity, alcohol, cigarette smoking, high cholesterol or high fat diets, and other harmful lifestyle regimens can lead to the formation of chronic ER stress and IRE1α activation (115-117). It will be interesting to investigate whether STING protein or downstream immune signaling is also impaired in these diseases. I showed that *Tollip*$^{-/-}$ completely rescued STING-mediated autoinflammatory disease in *Trex1*$^{-/-}$ mice. Targeting resting-state STING protein level through the TOLLIP-IRE1α-lysosome pathway may be a novel therapeutic strategy for STING-mediated diseases.

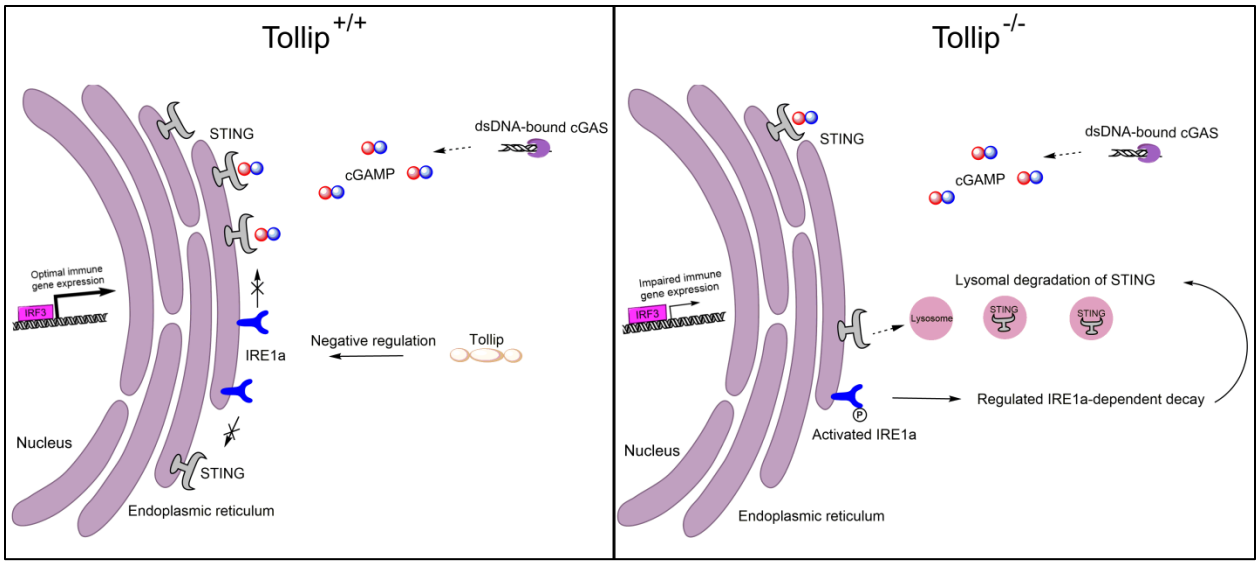

Figure 3.6: TOLLIP-mediated regulation of STING
A model of how the STING-dependent immune response occurs between *Tollip*$^{+/+}$ and *Tollip*$^{-/-}$cells.

In *Tollip*$^{+/+}$ cells, TOLLIP acts as negative regulator of the IRE1α UPR effector through an undefined mechanism. This negative regulation restrains sustained activation of IRE1α, preventing its effector function from negatively regulating STING protein. When 2'3'-cGAMP is in the cytosol, there exists an optimal amount of STING protein which can mediate a robust immune response.

Tollip$^{-/-}$ cells display activation of IRE1α RNase activity. Activation of this effector function leads to a lysosomal-dependent degradation of resting-state STING protein. STING-dependent signaling is impaired in this genotype due to a sub-optimal amount of basal STING protein.

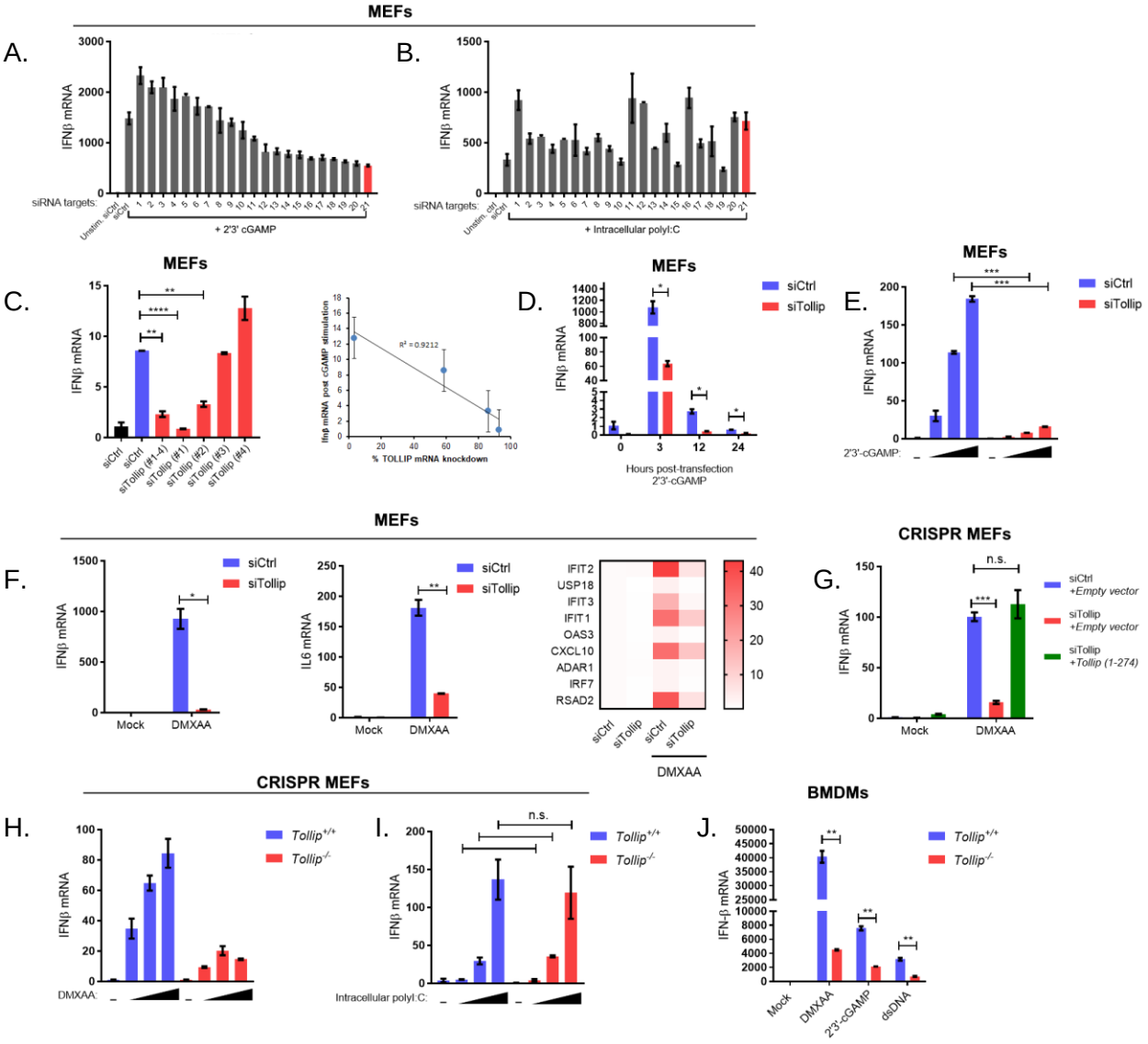

Figure 3.1: *Tollip* deficiency impairs STING-mediated signaling.
(A and B) Arrayed siRNA screen which 21 different gene targets were knocked down (KD) in MEFs. Quantitative RT-PCR (qRT-PCR) expression of *Ifnβ* mRNA following cGAMP stimulation (2μg/ml) for 5 hrs **(A)** or intracellular polyI:C (1μg/ml) for 5 hrs **(B).** **(C)** Expression of *Ifnβ* mRNA following cGAMP-stimulation (2μg/ml) for 5 hrs of KD MEFs with 4 distinct siRNA sequences targeting *Tollip*. Cells with greater *Tollip* KD had greater impairment in *Ifnβ* mRNA expression. **(D)** qRT-PCR of *Ifnβ* mRNA in *Tollip* KD MEFs stimulated with cGAMP (2μg/ml) over a 24-hour timecourse. **(E)** qRT-PCR of *Ifnβ* mRNA in *Tollip* KD MEFs stimulated with a dose-curve of cGAMP (0, 2, 3, 5μg/ml) for 5hrs. **(F)** qRT-PCR of *Ifnβ, Il6,* and *ISG* mRNA in *Tollip* KD MEFs stimulated with STING agonist DMXAA (50μg/ml) for 2hrs. **(G)** qRT-PCR of *Ifnβ* in *Tollip* KD cells expressing an empty vector or siRNA-resistant *Tollip* plasmid. Cells were stimulated with DMXAA (50μg/ml) for 2hrs. **(H)** *Tollip*$^{+/+}$ or *Tollip*$^{-/-}$ LentiCRISPR MEFs were stimulated with a dose-curve of DMXAA (0, 1, 10, 100μg/ml) for 2 hrs and assessed for expression of *Ifnβ* mRNA with qRT-PCR. **(I)** Same as in (H) but cells were stimulated with dose-curve of intracellular polyI:C (0, 0.01, 0.1, 1.0, 5.0, 10.0 ng/ml) for 5hrs. **(J)** Bone marrow-derived macrophages (BMDMs) from *Tollip*$^{+/+}$ or *Tollip*$^{-/-}$ cells were stimulated with intracellular dsDNA (1μg/ml) cGAMP (2μg/ml) or DMXAA (50μg/ml) and *Ifnβ* mRNA was measured with qRT-PCR*, $P < 0.05$; **, $P < 0.01$; ***, $P < 0.001$; and ****, $P < 0.0001$. Data are representative of at least three independent experiments. Error bars represent the SEM. Unpaired Student's t test (C–F).

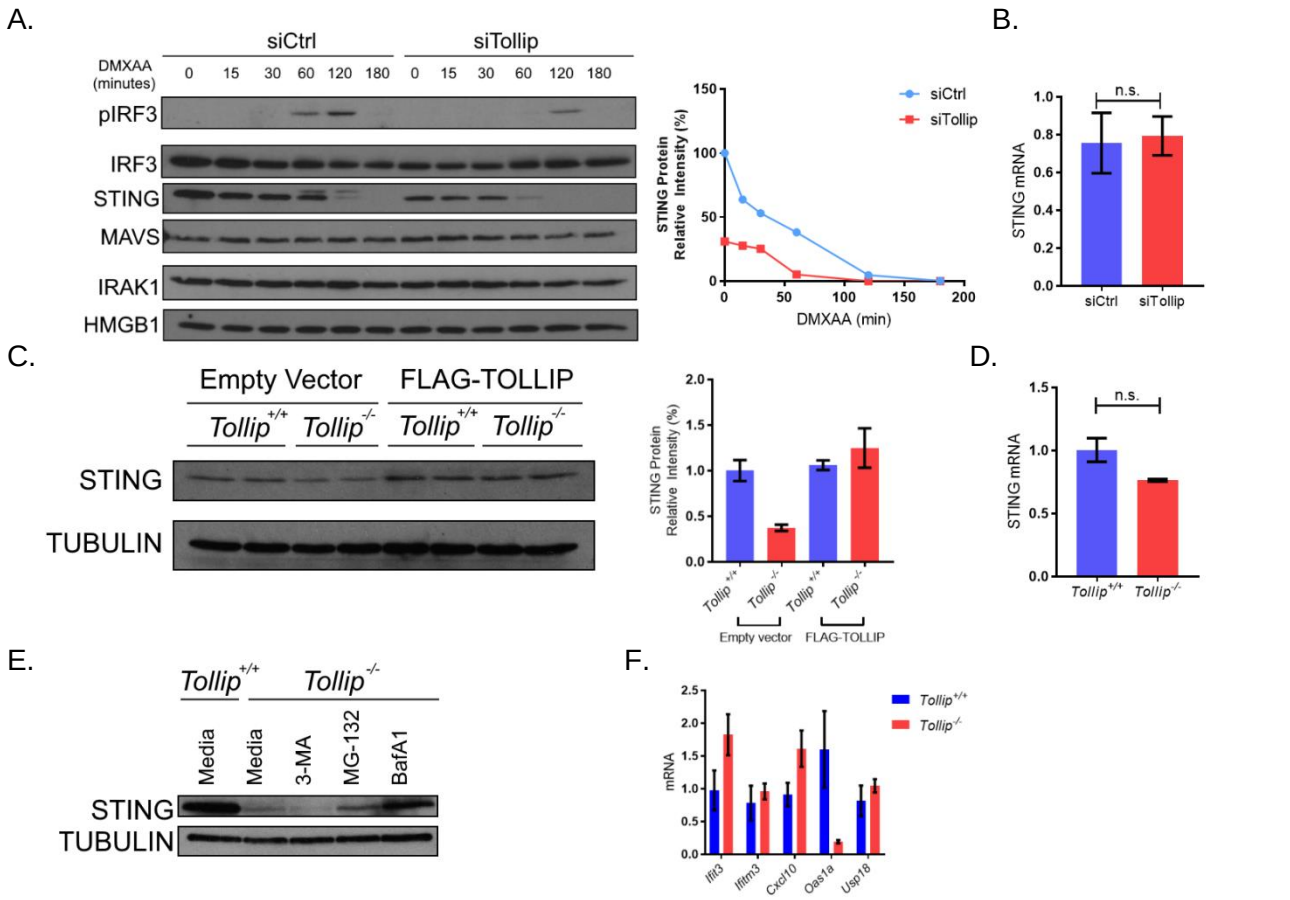

Figure 3.2: TOLLIP antagonizes basal lysosomal-mediated degradation of STING.
(A) Western blot of scrambled control or Tollip KD cells stimulated with DMXAA (50μg/ml) for indicated time points. Relative intensity of STING protein bands quantified on the right. **(B)** qRT-PCR measurement of basal *Sting* mRNA in scrambled control siRNA or *Tollip* KD cells. **(C)** *Tollip*$^{+/+}$ and *Tollip*$^{-/-}$ LentiCRISPR MEFs were stably transduced for stable expression of empty retroviral vector or retroviral-encoded FLAG-TOLLIP. Relative protein band intensity quantification on the right. **(D)** qRT-PCR measurement of basal *Sting* mRNA in *Tollip*$^{+/+}$ and *Tollip*$^{-/-}$ MEFs. **(E)** Western blot of *Tollip*$^{+/+}$ and *Tollip*$^{-/-}$ MEFs treated overnight with 3-MA (5mM), MG-132(5μM) and BafA1(0.5μM). **(F)**. qRT-PCR measurement of basal ISG mRNA in *Tollip*$^{+/+}$ and *Tollip*$^{-/-}$ MEFs. Error bars represent the SEM. Unpaired Student's t test (B, D).

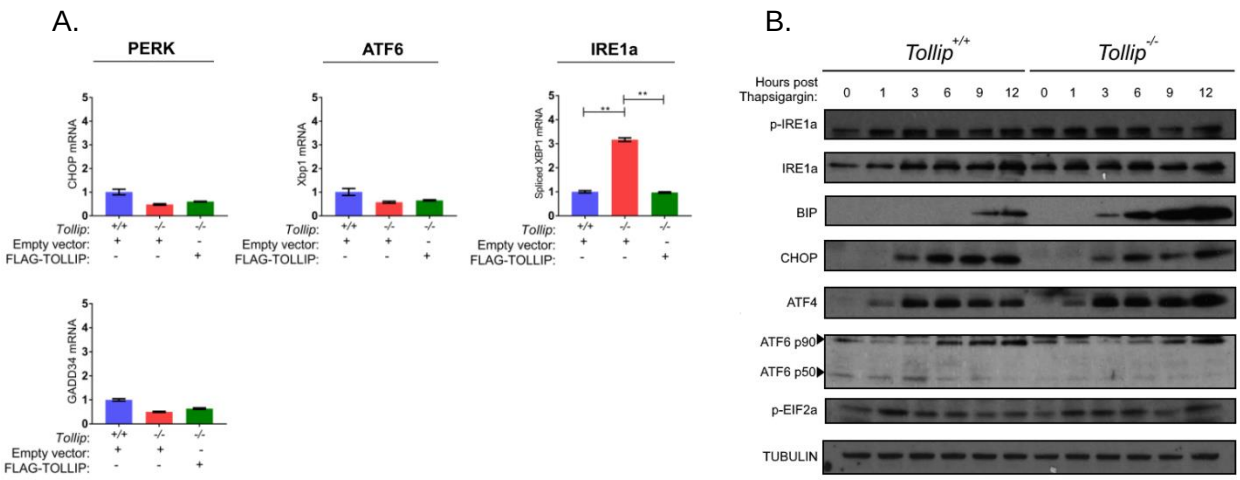

Figure 3.3: *Tollip*$^{-/-}$ cells display selective activation of IRE1α
(A) qRT-PCR measurement of basal UPR-dependent genes in *Tollip*$^{+/+}$ and *Tollip*$^{-/-}$ MEFs stably transduced with retroviral empty vector or retroviral-encoded FLAG-TOLLIP. **(B)** Western blot of *Tollip*$^{+/+}$ and *Tollip*$^{-/-}$ MEFs treated with thapsigargin (500nM) for indicated time points. Error bars represent the SEM. *, $P < 0.05$; **, $P < 0.01$; ***, $P < 0.001$; and ****, $P < 0.0001$ Unpaired Student's t test (A).

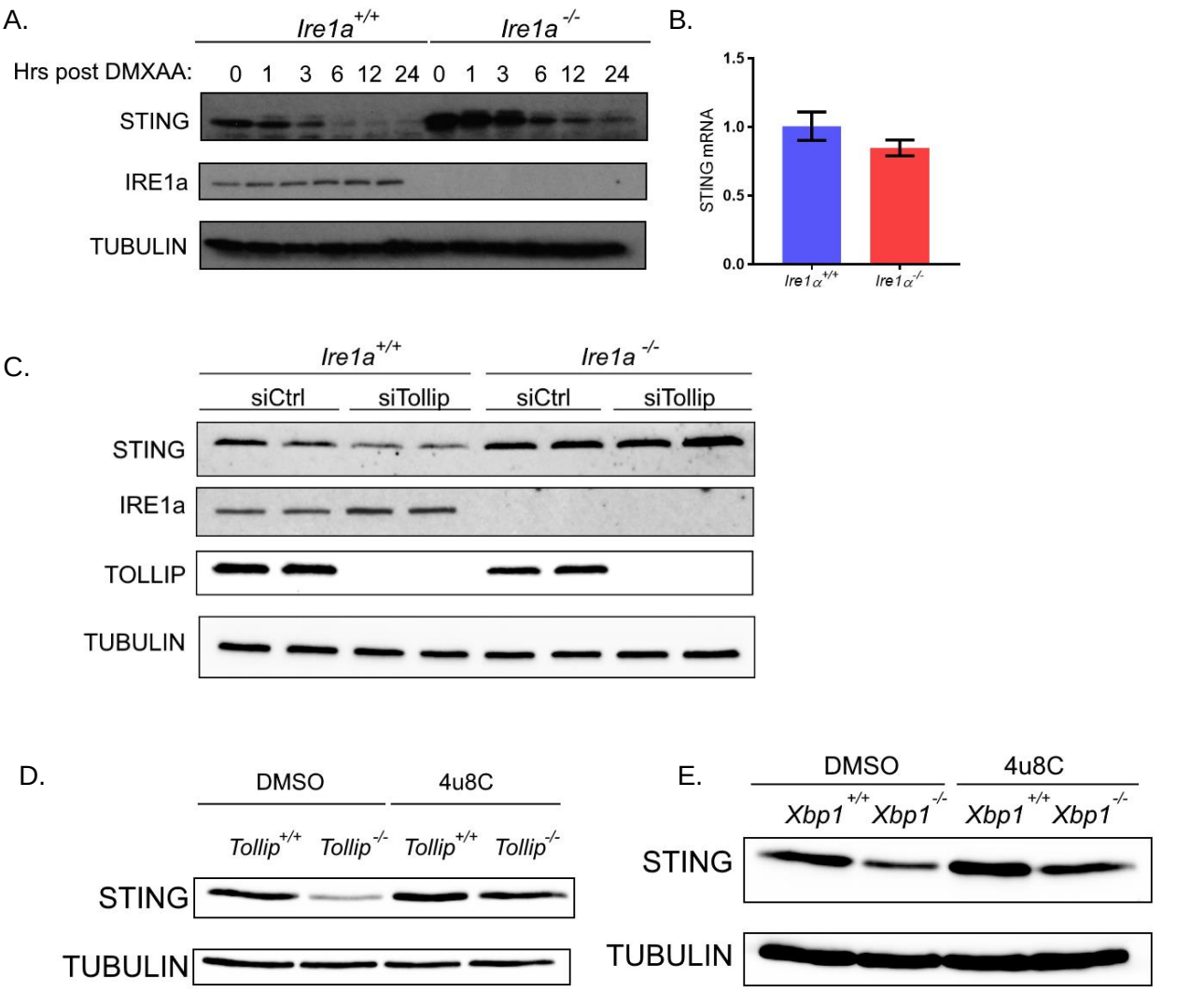

Figure 3.4: IRE1α regulates STING protein levels
(A) Western blot of *Ire1α*$^{+/+}$ and *Ire1α*$^{-/-}$ MEFs stimulated with DMXAA (10μg/ml) for indicated time points. **(B)** qRT-PCR measurement of basal *Sting* mRNA in *Ire1α*$^{+/+}$ and *Ire1α*$^{-/-}$ MEFs. **(C)** Western blot of *Ire1α*$^{+/+}$ and *Ire1α*$^{-/-}$ MEFs after KD with scrambled control siRNA or siTollip. **(D)** Western blot of *Tollip*$^{+/+}$ and *Tollip*$^{-/-}$ MEFs treated overnight with IRE1α inhibitor 4μ8C (100μM). **(E)** Western blot of *Xbp1*$^{+/+}$ and *Xbp1*$^{-/-}$ MEFs treated with 4μ8C (100μM) overnight. Data are representative of at least three independent experiments. Error bars represent the SEM. Unpaired Student's t test (B).

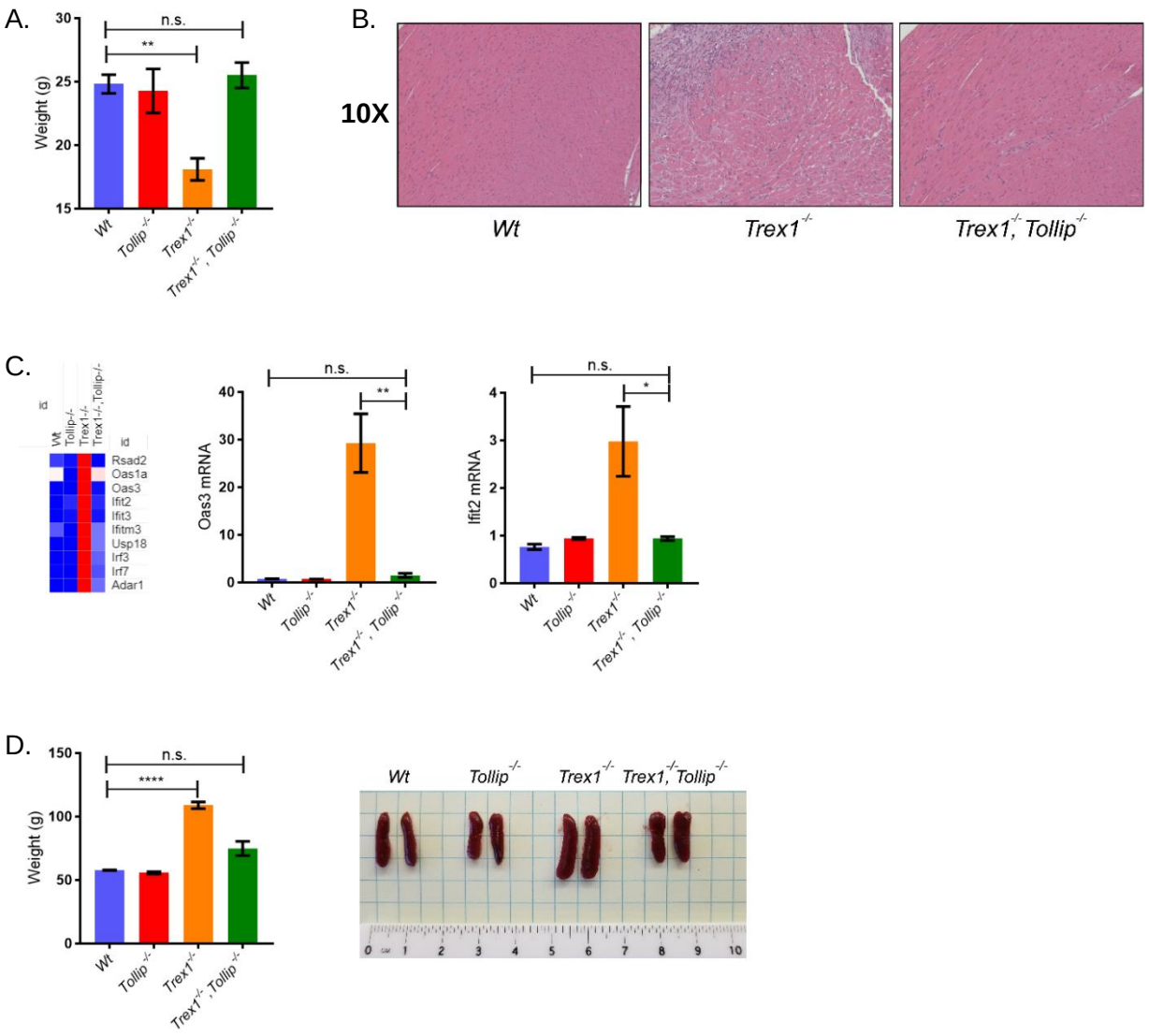

Figure 3.5: *Tollip*$^{-/-}$ ameliorates symptoms of autoinflammatory disease in *Trex1*$^{-/-}$ mice
(A) Weights of mice of indicated genotypes at 16 weeks. **(B)** H&E-stained hearts from 16 week old mice of indicated genotypes, with blue indicating infiltrating leukocytes. **(C)** Heatmap of ISGs from BMDMs of indicated genotypes with qRT-PCR quantification of representative genes to right. **(D)** Spleen weights of 16 week old mice with representative images to right. Error bars represent the SEM. *, $P < 0.05$; **, $P < 0.01$; ***, $P < 0.001$; and ****, $P < 0.0001$Unpaired Student's t test (A-D).

CHAPTER FOUR

CONCLUDING REMARKS

The cGAS-STING signaling pathway is vital in the sensing of intracellular DNA from bacteria or viruses (21, 22). Intricate regulation of this pathway allows optimal immune responses while also preventing harmful tissue destruction arising from overt inflammation. Dysregulation of the cGAS-STING pathway or its chronic activation has the potential to instigate auto-inflammatory and/or autoimmune diseases (59).

I have identified the involvement of the cGAS-STING pathway in the development of RNASEH2-mutant mediated AGS. During loss of function of RNASEH2, self-nucleic acid species activate the cGAS-STING pathway. My findings have also been confirmed by others using another RNASEH2 knock-in mouse model (118). These studies suggest cGAS activation during RNASEH2 deficiency depends on the sensing of self-DNA derived from nuclear bodies termed micronuclei (119-120). Work by others has shown that cGAS can enter the nuclei during cellular migration through tight junctions (121). Cells traversing through spaces smaller than 5 μm apart undergo a nuclear breakdown which permits cGAS to shuttle into the nucleus and bind to genomic DNA. As the membrane of micronuclei may be less intact compared to the nucleus, it may allow cGAS to access a pool of nuclear DNA and bind to ligands in a non-specific manner.

The micronuclei model is difficult to completely distinguish from the proposed role for RNase H2 in regulating retrotransposition of endogenous retroelements. Either cytosolic or nuclear RNase H2 could play a role in degrading the RNA: DNA hybrids of retroelements such as LINE-1 elements. In other work describing the dysregulation of LINE-1 or other

retroelements, it has been noted that genotoxicity can arise following the reintegration of retroelements within sites of the genome (137). This genotoxicity can potentially promote the formation of micronuclei in *Rnaseh2*-deficient cells, while also leading to the additional source of immunogenic cGAS ligands in the form of retroelement-derived nucleic acids. Regardless of the source of immunogenicity during *Rnaseh2*-deficiency, multiple bodies of work now implicate the cGAS-STING pathway in this subtype of AGS.

From a basic science standpoint, a lingering question is why disease hallmarks of AGS differ between humans and their respective mouse models. AGS patients have severe destruction of the CNS, while all mouse models of AGS fail to develop CNS tissue damage (64-67, 73, 78, 80, 81). Genetic diversity of AGS patients and differential brain development in human and mice are possibilities. Another interesting possibility is differences in human and mouse cGAS. Human cGAS contains a nuclear localization signal, while mouse cGAS does not (57, 122). This difference highlights one of many key species differences in the innate immune system between mice and humans. Does human cGAS have an enhanced ability to enter nuclear or micro-nuclear bodies in order to sense nucleic acids as compared to mouse cGAS? If true, this more accessible nuclear entrance may allow for higher induction of type I IFNs and ISGs within human cells.

Regardless of the discrepancies between human patients and mouse models of disease, it is imperative to develop inhibitors for innate immune sensors involved in AGS. Current work implicates MDA5-MAVS signaling as the instigator of *Ifih1*- and *Adar1*-mutant mediated AGS, while cGAS-STING initiates *Trex1*-, *Samhd1*-, and *Rnase2a/b/c*-mutant mediated AGS (Figure 4.1). Pharmacological inhibition of cGAS or STING in the *Trex1*$^{-/-}$ mouse model shows promise

(123), as both inhibitors ameliorated symptoms of *Trex1*$^{-/-}$-mediated disease. Clinical trials with these and future inhibitors in human patients hold promise.

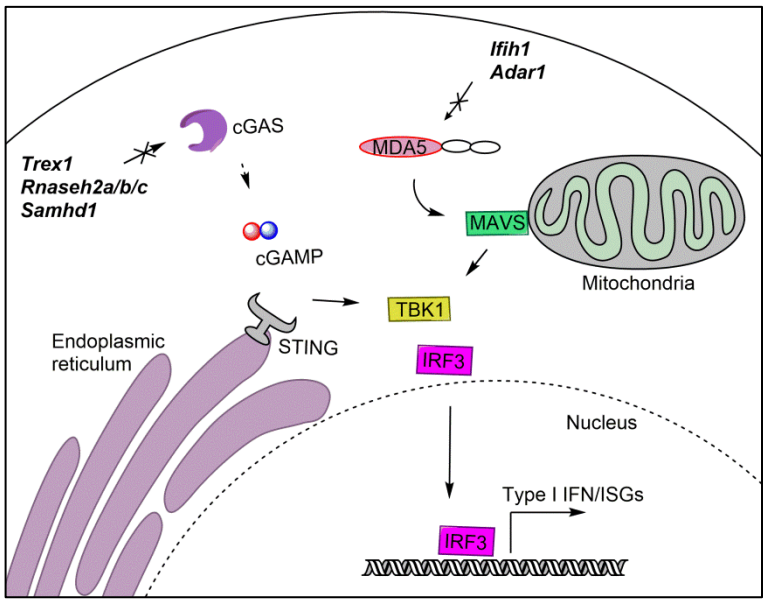

Figure 4.1: Immune pathways active in AGS
A model of how AGS subtypes develop. The cGAS-STING pathway is responsible for ISG upregulation in mouse models of AGS subtypes mediated by loss-of-function mutations in the *Trex1*, *Rnaseh2a/b/c*, and *Samhd1* genes. The MDA5-MAVS pathway is responsible for AGS in loss-of-function mutations in *Adar1* and in gain-of-function mutations of *Ifih1*.

A motivating force in my studies has been to further unravel regulators of the cGAS-STING pathway so that novel therapeutic inhibitors of this pathway may be considered for development. I had identified TOLLIP as a regulator of STING signaling, as it normally maintains resting-state STING protein level by preventing degradation through the lysosomes. TOLLIP does so through its regulation of an ER-associated protein, IRE1α. Chronic activation of IRE1α diminishes STING protein levels, thereby impairing STING-mediated signaling in response to dsDNA, cyclic dinucleotides and STING agonist DMXAA.

My data also implicates a possibility of impaired STING signaling in certain neurodegenerative disease. TOLLIP plays a critical role in removing Huntington's disease-linked polyQ proteins in the cell. Although it is technically challenging to detect endogenous polyQ protein in *Tollip*$^{-/-}$ mice, *Tollip*$^{-/-}$ has been shown to cause accumulation of β-amyloid and α-synuclein and promote neurodegenerative disease when crossed to *ApoE*$^{-/-}$ mice (138). PolyQ

protein exerts cytotoxicity through entrapment of ER chaperones, thus causing ER stress (139). The *Tollip*$^{-/-}$ mice do not exhibit any signs of neurodegeneration or other pathological symptoms, and I speculate that the mice are healthy due to undetectable amounts of ER stress. *Tollip*-deficient cells, rather than demonstrating a quantifiable induction of the UPR, undergo a measureable activation of IRE1α. The molecular mechanism as to how this selective activation of the IRE1α branch occurs remains unresolved but will be important to characterize in subsequent work.

Different neurodegenerative protein aggregates are believed to trigger different cellular responses, raising an intriguing possibility that STING signaling may be impaired in certain neurodegenerative diseases such as HD. STING has also been implicated in Parkinson's disease and *NGLY1* disease through sensing mitochondrial DNA (140, 141). These findings together highlight an expanding role of STING signaling in autoimmune and neurodegenerative diseases. I have demonstrated that *Tollip*$^{-/-}$ rescued STING-mediated autoimmune disease in *Trex1*$^{-/-}$ mice. Targeting resting-state STING protein level through the TOLLIP-IRE1α-lysosome pathway may be a novel therapeutic strategy for STING-mediated diseases.

These findings represent another example of a crosstalk between stress responses and the innate immune system. Many studies have focused on the immune pathways directly activated as a result of cellular stress. For example, in the absence of the RNA exosome, SKIV2L, ER stress has been shown to activate a RIG-I-MAVS dependent pathway (124). An important question which has not been examined in as much detail is how do these cellular stressors affect other innate signaling pathways? This is an important area to pursue in future research as diseases are complex and their etiologies may lie at the intersection of several signaling pathways. For

example, with the findings from my work, one disease to pursue this concept in is cancer. In the non-stressed physiological environment, senescence is allowed to occur through the sensing of self-DNA by the cGAS-STING pathway (125, 126). Chronic activation of IRE1α through ER stress may impair this cGAS-STING signaling response. This impairment in signaling may allow for the proliferation of oncogenic cells, and the formation of tumors. Such hypotheses are important to examine in future work.

As early as 2004, it was observed that DNA virus infections can activate an innate immune response independently of the extracellular-DNA sensor, TLR9 (127). This observation motivated the pursuit to identify the DNA-sensing equivalent of the RIG-I-MAVS pathway, largely accelerated in 2008 with the discovery of the DNA-sensing adapter STING and climaxed in late 2012 with the discovery of cytosolic DNA sensor cGAS (21, 128). Since that time, our understanding of the immune sensing of the fundamental building blocks of life has grown exponentially, with reports of its involvement in viral and bacterial infections, auto-inflammatory and autoimmune diseases, and also cancer. Work in this field will continue to grow as we begin considering the roles of this pathway in non-immune roles, such as regulation of apoptosis, cellular proliferation, autophagy, and many more yet unappreciated phenomena.

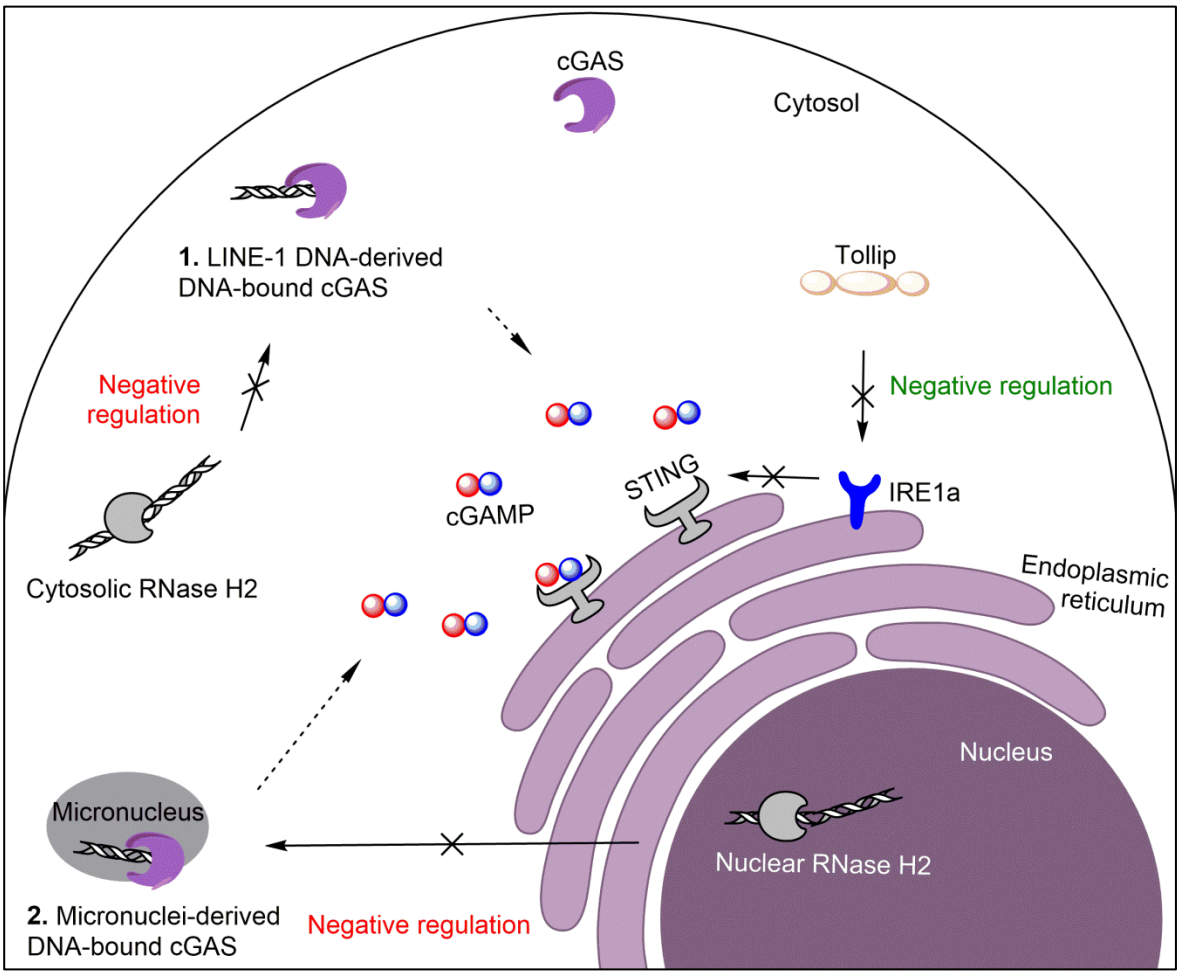

Figure 4.2: Regulation of the cGAS-STING pathway in health and disease
A model of how positive and negative regulators can influence the cGAS-STING pathway.

TOLLIP acts as a positive regulator of the STING pathway through **negative regulation** of the UPR effector IRE1α. TOLLIP restrains constitutive IRE1α activation, thereby preventing STING from being degraded through a lysosomal pathway. The molecular mechanism of TOLLIP regulating IRE1α remains undefined; however, it may be through direct regulation of the effector or through degradation of unfolded proteins which may activate IRE1α.

RNase H2 acts as a negative regulator of the cGAS-STING pathway through the **negative regulation** of immunogenic DNA which can appear in the cytosol. This DNA remains a topic of debate as it may come from the accumulation of endogenous retroelements in the cytosol of cells in the absence of RNase H2. Cytosolic DNA may also arise as a consequence of DNA damage which occurs in the absence of RNase H2. The sources of DNA remain a contested topic; however, a pivotal role of cGAS in detecting this DNA is well-established.

BIBLIOGRAPHY

1. Pradeu T., Jaeger S., Vivier E. 2013. The speed of change: towards a discontinuity theory of immunity? *Nature Reviews Immunology.* Vol 13(10): 764-9

2. Pradeu T., Vivier E. 2016. The discontinuity theory of immunity. *Science Immunology*. Vol 1(1).

3. Medzhitov R. 2007. Recognition of microorganisms and activation of the immune response. *Nature.* Vol 449: 819-826.

4. Goubau D., Deddouche S., Reis e Sousa C. 2013. Cytosolic sensing of viruses. *Immunity*. Vol 38: 855-869.

5. Hartmann G. Nucleic acid immunity. 2017. *Advances in Immunology.* Vol 133: 121-169.

6. Schneider WM, Chevillotte MD, Rice CM. 2014. Interferon-stimulated genes: a complex web of host defenses. *Annual Reviews Immunology* Vol 32: 513–45.

7. Schoggins JW, Rice CM. 2011. Interferon-stimulated genes and their antiviral effector functions. *Current Opinion in Virology*. Vol 1: 519–525.

8. Schoggins JW. 2014. Interferon-stimulated genes: roles in viral pathogenesis. *Current Opinion in Virology*. Vol 6: 40–46.

9. Poltorak A., He X., Smirnova I., Liu M., Huffel CV., Du X., Birdwell D., Alejos E., Silva M., Galanos C., Freudenberg M., Ricciardi-Castagnoli P., Layton B., Beutler B. 1998. Defective LPS signaling in C3H/HeJ and C57BL/10ScCr mice: mutations in Tlr4 gene. *Science*. Vol 282: 2085-2088.

10. Diebold S., Kaisho T., Hemmi H., Akira S., Reis e Sousa C. 2004. Innate Antiviral Responses by means of TLR7-mediated recognition of single-stranded RNA. *Science*. Vol 303: 1529-1531.

11. Heil F., Hemmi H., Hochrein H., Ampenberger F., Kirschning C., Akira S. Lipford G., Wagner H. Bauer S. 2004. Species-specific recognition of single-stranded RNA via Toll-like receptor 7 and 8. *Science*. Vol 303: 1526-1529.

12. Gehrig S., Eberle M., Botschen F.,Rimbach K., Eberle F., Eigenbrod T., Kaiser S., Holmes WM., Erdmann VA, Sprinzl M., Bec G., Keith G., Dalpke AH., Helm M. 2012. Identification of modifications in microbial, native tRNA that suppress immunostimulatory activity. *The Journal of Experimental Medicine*. Vol. 209: 225-233.

13. Hemmi H., Takeuchi O., Kawai T., Kaisho T., Sato S., Sanjo H., Matsumoto M., Katsuaki H., Wagner H., Takeda K., Akira S. 2000. A Toll-like receptor recognizes bacterial DNA. *Nature.* Vol 408: 740-745.

14. Rigby RE., Webb LM., Mackenzie KJ., Li Y., Leitch A., Reijns MA., Lundie RJ., Revuelta A., Davidson DJ, Diebold S., Modis Y., MacDonald AS., Jackson AP. 2014. RNA:DNA hybrids are a novel molecular pattern sensed by TLR9. *The EMBO Journal.* Vol 33: 542-558.

15. Kell AM., Gale MJ. 2015. RIG-I in RNA virus recognition. *Virology*. Vol 479-480: 110–121.

16. Chiang C., Gack MU. 2017. Post-translational control of intracellular pathogen sensing pathways. *Trends in Immunology*. Vol 38: 39-52.

17. Xu X., Wan H., Nie L., Shao T., Xiang L., Shao J. 2018. RIG-I: a multifunctional protein beyond a pattern recognition receptor. *Protein Cell.* Vol 9: 246–253.

18. Pichlmair A., Schulz O., Tan C., Rehwinkel J., Kato H., Takeuchi O., Akira S., Way M., Schiavo G., Reis e Sousa C. 2009. Activation of MDA5 requires higher-order RNA structures generated during virus infection. *Journal of Virology.* Vol 83: 10761–10769.

19. Gack MU., Shin YC., Joo C., Urano T., Liang C., Sun L., Takeuchi O., Akira S., Chen ZJ., Inoue S., Jung JU. 2007.TRIM25 RING-finger E3 ubiquitin ligase is essential for RIG-I-mediated antiviral activity. *Nature.* Vol 446: 916-921.

20. Liu S., Cai X., Wu J., Cong Q., Chen X., Li T., Du F., Ren J., Wu Y., Grishin N., Chen ZJ. 2015. Phosphorylation of innate immune adaptor proteins MAVS, STING, and TRIF induces IRF3 activation. *Science.* Vol 347.

21. Sun L., Wu J., Du F., Chen X., Chen ZJ. 2012. Cyclic GMP-AMP synthase is a cytosolic DNA sensor that activates the type I interferon pathway. *Science*. Vol 339: 786-791.

22. Gray EE., Winship D., Snyder JM., Child SJ., Geballe AP. Steston DB. 2016. The AIM2-like receptors are dispensable for the interferon response to intracellular DNA. *Immunity.* Vol 45: 255–266.

23. Civril F., Deimling T., de Oliveira Mann CC., Ablasser A., Moldt M., Witte G., Hornung V., Hopfner K. 2013. Structural mechanism of cytosolic DNA sensing by cGAS. *Nature*. Vol 498: 332-337.

24. Zhang X., Wu J., Du F., Xu H., Sun L., Chen Z., Brautigam CA., Zhang X., Chen ZJ. 2014. The cytosolic DNA sensor cGAS forms an oligomeric complex with DNA and undergoes switch-like conformational changes in the activation loop. *Cell Reports*. Vol 6: 421–430.

25. Wu J., Sun L., Chen X., Du F., Shi H., Chen C. Chen ZJ. 2013. Cyclic GMP-AMP is an endogenous second messenger in innate immune signaling by cytosolic DNA. *Science*. Vol 339: 826-830.

26. Ablasser A., Schmid-Burgk JL., Hemmerling I., Horvath GL., Schmidt T., Latz E., Hornung V. 2013. Cell intrinsic immunity spreads to bystander cells via the intercellular transfer of cGAMP.Vol 503: 530-536.

27. Hansen K., Prabakaran T., Laustsen A., Jørgensen SE., Rahbæk SH., Jensen SB., Nielsen R., Leber JH., Decker T., Horan KA., Jakobsen MR., Paludan SR. 2014. Listeria monocytogenes induces IFNb expression through an IFI16-, cGAS- and STING-dependent pathway. *The EMBO Journal.* Vol 33: 1654-1666.

28. Gao D., Wu J., Wu Y., Du F., Aroh C., Yan N., Sun L., Chen ZJ. 2013. Cyclic GMP-AMP synthase is an innate immune sensor of HIV and other retroviruses. *Science*. Vol 341: 903-906.

29. Li X., Wu J., Gao D., Wang H., Sun L., Chen ZJ. 2013. Pivotal roles of cGAS-cGAMP signaling in antiviral defense and immune adjuvant effects. *Science* Vol 341: 1390-1394

30. Hartlova A., Erttmann SF., Raffi FA., Schmalz AM., Resch U., Anugula S., Lienenklaus S., Nilsson LM., Kroger A., Nilsson JA., Ek T., Weiss S., Gekara NO. 2015. DNA damage primes the type I interferon system via the cytosolic DNA sensor STING to promote anti-microbial innate immunity. *Immunity*. Vol 42: 332–343.

31. Burdette DL., Monroe KM., Sotelo-Troha K., Iwig JS., Eckert B., Hyodo M., Hayakawa Y., Vance RE. 2011. STING is a direct innate immune sensor of cyclic di-GMP. Vol 478: 515-519.

32. Margolis SR., Wilson SC., Vance RE. 2017. Evolutionary origins of cGAS-STING signaling. *Trends in Immunology*. Vol 38: 733-743.

33. Abe T., Barber GN. 2014. Cytosolic-DNA-mediated, STING-dependent proinflammatory gene induction necessitates canonical NF-κB activation through TBK1. *Journal of Virology*. Vol 88: 5328–5341.

34. Saitoha T., Fujitac N., Hayashic T., Takaharaa K., Satoha T., Leea H., Matsunagac K., Kageyamac S., Omoric H., Nodac T., Yamamotoe N., Kawaia T. Ishiia K., Takeuchia O., Yoshimoric T., Akiraa S. 2009. Atg9a controls dsDNA-driven dynamic translocation of STING and the innate immune response. *PNAS*. Vol 106: 20842–20846.

35. Gonugunta VK., Sakai T., Pokatayev V., Yang K., Wu J., Dobbs N., Yan N. 2017. Trafficking-Mediated STING Degradation Requires Sorting to Acidified Endolysosomes and Can Be Targeted to Enhance Anti-tumor Response. *Cell Reports* Vol 21: 3234–3242.

36. Gaidt MM., Ebert TS., Chauhan D., Ramshorn K., Pinci F., Zuber S., O'Duill F., Schmid-Burgk JL., Hoss F., Buhmann R., Wittman G., Latz E., Subklewe M., Hornung V. 2017. The DNA inflammasome in human myeloid cells is initiated by a STING-cell death program upstream of NLRP3. *Cell.* Vol 171: 1110–1124.

37. Seo GJ., Yang A., Tan B., Kim S., Liang Q., Choi Y., Yuan W. Feng P., Park H., Jung JU. 2015. Akt kinase-mediated checkpoint of cGAS DNA sensing pathway. *Cell Reports* Vol 13: 440–449.

38. Xia P., Ye B., Wang S., Zhu X., Du Y., Xiong Z., Tian Y., Fan Z. 2016. Glutamylation of the DNA sensor cGAS regulates its binding and synthase activity in antiviral immunity. *Nature Immunology*. Vol 17: 369-378.

39. Hu M., Yang Q., Xie X., Liao C., Lin H., Liu T., Yin L., Shu H. 2016. Sumoylation promotes the stability of the DNA sensor cGAS and the adaptor STING to regulate the kinetics of response to DNA virus. *Immunity* Vol 45: 555–569.

40. Seo GJ., Kim C., Shin W., Sklan EH., Eoh H., Jung JU. 2018. TRIM56-mediated monoubiquitination of cGAS for cytosolic DNA sensing. *Nature Communications*. Vol 9: 1-13.

41. Liu Z., Zhang Z., Cai H., Zhao M., Mao J., Dai J., Xia T., Zhang X., Li T. 2018. RINCK-mediated monoubiquitination of cGAS promotes antiviral innate immune responses. *Cell and Bioscience*. Vol 8: 1-9.

42. Wang Q., Huang L., Hong Z., Lv Z., Mao Z., Tang Y., Kong X., Li S., Cui Y., Liu H., Zhang L., Zhang X., Jiang L., Wang C., Zhou Q. 2017.The E3 ubiquitin ligase RNF185 facilitates the cGAS-mediated innate immune response. *PLOS Pathogens*. Vol 13: 1-25.

43. Chen M., Meng Q., Qin Y., Liang P., Tan P., He L., Zhou Y., Chen Y., Huang J., Wang R., Cui J. 2016. TRIM14 inhibits cGAS degradation mediated by selective autophagy receptor p62 to promote innate immune responses. *Molecular Cell*. Vol 64: 105-119.

44. Wang Y., Ning X., Gao P., Wu S., Sha M., Lv M., Zhou X., Gao J., Fang R., Meng G., Su X., Jiang Z. 2017. Inflammasome Activation Triggers Caspase-1-Mediated Cleavage of cGAS to Regulate Responses to DNA Virus Infection. *Immunity*. Vol 46: 393–404.

45. Wang Q., Liu X., Cui Y., Tang Y., Chen W., Li S., Yu H., Pan Y., Wang C. 2014. The E3 ubiquitin ligase AMFR and INSIG1 bridge the activation of TBK1 kinase by modifying the adaptor STING. *Immunity*. Vol 41: 919–933.

46. Qin Y., Zhou M., Hu M., Hu Y., Zhang J., Guo L., Zhong B., Shu H. 2014. RNF26 temporally regulates virus-triggered type I interferon induction by two distinct mechanisms. *PLOS Pathogens*. Vol 10: 1-14.

47. Zhang J., Hu M., Wang Y., Shu H. 2012. TRIM32 protein modulates type I interferon induction and cellular antiviral response by targeting MITA/STING protein for K63-linked ubiquitination. *Journal of Biological Chemistry*. Vol 287: 28646-28655.

48. Tsuchida T., Zou J., Saitoh T., Kumar H., Abe T., Matsuura Y., Kawai T., Akira S. 2010. The ubiquitin ligase TRIM56 regulates innate immune responses to intracellular double-stranded DNA. *Immunity* Vol 33: 765–776.

49. Luo W., Li S., Li C., Lian H., Yang Q., Zhong B., Shu H. 2016. iRhom2 is essential for innate immunity to DNA viruses by mediating trafficking and stability of the adaptor STING. *Nature Immunology*. Vol 17: 1057-1066.

50. Zhang M., Zhang M., Zhang Q., Zhu G., Yuan L., Zhang D., Zhu Q., Yao J., Shu H., Zhong B. 2016. USP18 recruits USP20 to promote innate antiviral response through deubiquitinating STING/MITA. *Cell Research*. Vol 26: 1302-1319.

51. Zhong B., Zhang L., Lei C., Li Y., Mao A., Yang Y., Wang Y., Zhang X. 2009. The ubiquitin ligase RNF5 regulates antiviral responses by mediating degradation of the adaptor protein MITA. *Immunity* Vol 30: 397–407.

52. Li Q., Lin L., Tong Y., Liu Y., Mou J., Wang X., Wang X., Gong Y., Zhao Y., Liu Y., Zhong B., Dai L., Wei Y., Zhang H., Hu H. 2018. TRIM29 negatively controls antiviral immune response through targeting STING for degradation. *Cell Discovery*. Vol 4: 1-13.

53. Xing J., Zhang A., Zhang H., Wang J., Li XC., Zeng Mu., Zhang Z. 2017. TRIM29 promotes DNA virus infections by inhibiting innate immune response. *Nature Communications.* Vol 8: 1-12.

54. Wang Y., Lian Q., Yang B., Yan S., Zhou H., He L., Lin G., Lian Z., Jiang Z., Sun B. 2015. TRIM30α is a negative-feedback regulator of the intracellular DNA and DNA virus-triggered response by targeting STING. *PLOS Pathogens*. Vol 6: 1-18.

55. Sun H., Zhang Q., Jing Y., Zhang M., Wang H., Cai Z., Liuyu T., Zhang Z., Xiong T., Wu Y., Zhu Q., Yao J., Shu H., Lin D., Zhong B. 2016. USP13 negatively regulates antiviral responses by deubiquitinating STING. *Nature Communications.* Vol 8: 1-13.

56. Mukai K., Konno H., Akiba T., Uemura T., Waguri S., Kobayashi T., Barber GN., Arai H., Taguchi T. 2016. Activation of STING requires palmitoylation at the Golgi. *Nature Communications.* Vol 7: 1-10.

57. Haag S., Gulen M., Reymond L., Gibelin A., Abrami L., Decout A., Heymann M., van der Goot G., Turcatti G., Behrendt R., Ablasser A. 2018. Targeting STING with covalent small-molecule inhibitors. *Nature*. Vol 559: 269-276.

58. Kotas ME., Medzhitov R. 2015. Homeostasis, inflammation, and disease susceptibility. *Cell* Vol 160: 816-827.

59. Crow YJ., Manel N. 2015. Aicardi–Goutières syndrome and the type I interferonopathies. *Nature Reviews Immunology*. Vol 15: 429-440.

60. Crow YJ, Chase DS, Lowenstein Schmidt J, Szynkiewicz M, Forte GM, Gornall HL, Oojageer A, Anderson B, Pizzino A, Helman G, Abdel-Hamid MS, Abdel-Salam GM, Ackroyd S, Aeby A, Agosta G, Albin C, Allon-Shalev S, Arellano M, Ariaudo G, Aswani V, Babul-Hirji R, Baildam EM, Bahi-Buisson N, Bailey KM, Barnerias C, Barth M, Battini R, Beresford MW, Bernard G, Bianchi M, Billette de Villemeur T, Blair EM, Bloom M, Burlina AB, Luisa Carpanelli M, Carvalho DR, Castro-Gago M, Cavallini A, Cereda C, Chandler KE, Chitayat DA, Collins AE, Sierra Corcoles C, Cordeiro NJ, Crichiutti G, Dabydeen L, Dale RC, D Arrigo S, De Goede CG, De Laet C, De Waele LM, Denzler I, Desguerre I, Devriendt K, Di Rocco M, Fahey MC, Fazzi E, Ferrie CD, Figueiredo A, Gener B, Goizet C, Gowrinathan NR, Gowrishankar K, Hanrahan D, Isidor B, Kara B, Khan N, King MD, Kirk EP, Kumar R, Lagae L, Landrieu P, Lauffer H, Laugel V, Piana RL, Lim MJ, Lin JS, Linnankivi T, Mackay MT, Marom DR, Marques Lourenc¸o C, McKee SA, Moroni I, Morton JE, Moutard M-L, Murray K, Nabbout R, Nampoothiri S, Nunez-Enamorado N, Oades PJ, Olivieri I, Ostergaard JR, Pe´rez-Duen˜as B, Prendiville JS, Ramesh V, Rasmussen M, Re´gal L, Ricci F, Rio M, Rodriguez D, Roubertie A, Salvatici E, Segers KA, Sinha GP, Soler D, Spiegel R, Stodberg TI, Straussberg R, Swoboda KJ, Suri M, Tacke U, Tan TY, te Water Naude J, Wee Teik K, Mary Thomas M, Till M, Tonduti D, Maria Valente E, Noel Van Coster R, van der Knaap MS, Vassallo G, Vijzelaar R, Vogt J, Wallace GB, Wassmer E, Webb HJ, Whitehouse WP, Whitney RN, Zaki MS, Zuberi SM, Livingston JH, Rozenberg F, Lebon P, Vanderver A, Orcesi S, Rice GI. 2015. Characterization of human disease phenotypes associated with mutations in TREX1, RNASEH2A, RNASEH2B, RNASEH2C, SAMHD1, ADAR, and IFIH1. *American Journal of Medical Genetics.* Vol 167A:296–312.

61. Dan J. Mazur DJ., Perrino FW. 1999. Identification and expression of the TREX1 and TREX2 cDNA sequences encoding mammalian 3-5 exonucleases. *Journal of Biological Chemistry.* Vol. 274: 19655–19660.

62. Crow YJ., Hayward BE., Parmar R., Robins P., Leitch A., Ali M., Black DN., Bokhoven HV., Brunner HG., Hamel BC., Corry PC., Cowan F., Frints SG., Klepper J., Livingston JH., Lynch SA., Massey RF., Francoi J., Michaud JL., Ponsot G., Voit T., Lebon P., Bonthron DT., Jackson AP., Barnes DE., Lindahl T. 2006. Mutations in the gene

encoding the 3-5 DNA exonuclease TREX1 cause Aicardi-Goutières syndrome at the AGS1 locus. *Nature Genetics.* Vol 38: 917-920.

63. Yang Y., Lindahl T., Barnes DE. 2007. Trex1 exonuclease degrades ssDNA to prevent chronic checkpoint activation and autoimmune disease. *Cell.* Vol 131: 873–886.

64. Gall A., Treuting P., Elkon KB., Loo Y., Gale MJ., Barber GN., Stetson DB. 2012. Autoimmunity initiates in nonhematopoietic cells and progresses via lymphocytes in an interferon-dependent autoimmune disease. *Immunity*. Vol 36: 120–131.

65. Gao D., Lia T., Lia X., Chen X., Lic Q., Wight-Carter M., Chen ZJ. 2015. Activation of cyclic GMP-AMP synthase by self-DNA causes autoimmune diseases. *PNAS.* E5699–E5705.

66. Ablasser A., Hemmerling I., Schmid-Burgk JL., Behrendt R., Roers A., Hornung V. 2014. TREX1 deficiency triggers cell-autonomous immunity in a cGAS-dependent manner. *The Journal of Immunology*. Vol 192: 5993-5997.

67. Gray EE., Treuting PM., Woodward JJ., Stetson DB. 2015. Cutting Edge: cGAS is required for lethal autoimmune disease in the Trex1-deficient mouse model of Aicardi–Goutières Syndrome. *The Journal of Immunology*. Vol 195:1939-1943.

68. Stetson DB., Ko JS., Heidmann T., Medzhitov R. 2008. Trex1 prevents cell-intrinsic initiation of autoimmunity. *Cell.* Vol 134: 587–598.

69. Goldston DC., Ennis-Adeniran V., Hedden JJ., Groom HCT., Rice GI., Christodoulou Evangelos., Walker PA., Kelly G., Haire LF., Yap MW., de Carvalho LPS., Stoye JP., Crow YJ., Taylor IA., Webb M. 2011. HIV-1 restriction factor SAMHD1 is a deoxynucleoside triphosphate triphosphohydrolase. *Nature.*Vol 480: 379-383.

70. Lahoussa H., Daddacha W., Hofmann H., Ayinde D., Logue EC., Dragin L., Bloch N., Maudet C., Bertrandt M., Gramberg T., Pancino G., Priet S., Canard B., Laguette N., Benkirane M., Transy C., Landau NR., Kim B., Margottin-Goguet F. 2012. SAMHD1 restricts the replication of human immunodeficiency virus type 1 by depleting the intracellular pool of deoxynucleoside triphosphates. *Nature Immunology*. Vol 13: 223-230.

71. Kane M., Zang TM., Rihn SJ., Zhang F., Kueck T., Alim M., Schoggins JW., Rice CM., Wilson SJ., Bieniasz PD. 2016. Identification of interferon-stimulated genes with antiretroviral activity. *Cell Host & Microbe.* Vol 20: 392–405.

72. Behrendt R., Schumann T., Gerbaulet A., Nguyen LA., Schubert N., Alexopoulou D., Berka U., Lienenklaus S., Peschke K., Gibbert K., Wittmann S., Lindemann D., Weiss S., Dahl A., Naumann R., Dittmer U., Kim B., Mueller W., Gramberg T., Roers A. 2013. Mouse

SAMHD1 has antiretroviral activity and suppresses a spontaneous cell-intrinsic antiviral response. *Cell Reports.* Vol 4: 689–696.

73. Maelfait J., Bridgeman A., Benlahrech A., Cursi C., Rehwinkel J. 2016. Restriction by SAMHD1 limits cGAS/STING-dependent innate and adaptive immune responses to HIV-1. *Cell Reports* Vol 16: 1492–1501.

74. Coquel F., Silva M., Techer H., Zadorozhny K., Sharma S., Nieminuszczy J., Mettling C., Dardillac E., Barthe A., Schmitz A., Promonet A., Cribier A., Sarrazin A., Niedzwiedz W., Lopez B., Costanzo V., Krejci L., Chabes A., Benkirane M., Lin Y., Pasaro P.2018. SAMHD1 acts at stalled replication forks to prevent interferon induction. *Nature*. Vol 557: 57-64.

75. Herzner A., Hagmann CA., Goldeck M., Wolter S., Kubler K., Wittmann S., Gramberg T., Andreeva L., Hopfner K., Mertens C., Zillinger T., Jin T., Xiao TS., Bartok E., Coch C., Ackermann D., Hornung V., Ludwig J., Barchet W., Hartmann G., Schlee M. 2015. Sequence-specific activation of the DNA sensor cGAS by Y-form DNA structures as found in primary HIV-1 cDNA. *Nature Immunology*. Vol 16: 1025-1035.

76. Kim U., Wang Y., Sanford T., Zeng Y., Nishikura K. 1994. Molecular cloning of cDNA for double-stranded RNA adenosine deaminase, a candidate enzyme for nuclear RNA editing. *PNAS.* Vol. 91: 11457-11461.

77. Patterson JB., Samuel CE. 1995. Expression and regulation by interferon of a double-stranded-RNA-specific adenosine deaminase from human cells: evidence for two forms of the deaminase. *Molecular and Cellular Biology.* Vol 15: 5376–5388.

78. Pestal K., Funk CC., Snyder JM., Price ND., Treuting PM., Stetson DB. 2015. Isoforms of RNA-editing enzyme ADAR1 independently control nucleic acid sensor MDA5-driven autoimmunity and multi-organ development. *Immunity* Vol 43: 933–944.

79. Rice GI., Kasher PR., Forte GMA., Mannion NM., Greenwood SM., Szynkiewicz M., Dickerson JE., Bhaskar SS., Zampini M., Briggs TA., Jenkinson EM., Bacino CA., Battini R., Bertini E., Brogan PA., Brueton LA., Carpanelli M., De Laet C., de Lonlay P., del Toro M., Desguerre I., Fazzi E., Garci-Cazorla A., Heiberg A., Kawaguchi M., Kumar R., Lin JP., Lourenco CM., Male AM., Marques W., Mignot C., Olivieri I., Orcesi S., Prabhakar P., Rasmussen M., Robinson RA., Rozenberg F., Schmidt JL., Steindl K., Tan TY., van der Merwe W., Vanderver A., Vassallo G., Wakeling EL., Wassmer E., Whittaker E., Livingston JH., Lebon P., Suzuki T., McLaughlin PJ., Keegan LP., O'Connell MA., Lovell SC., Crow YJ. 2012. Mutations in ADAR1 cause Aicardi-Goutières syndrome associated with a type I interferon signature. *Nature Genetics.* Vol 44: 1243-1250.

80. Liddicoat BJ., Piskol R., Chalk AM., Ramaswami G., Higuchi M., Hartner JC., Li JB., Seeburg PH., Walkley CR. 2015. RNA editing by ADAR1 prevents MDA5 sensing of endogenous dsRNA as nonself. *Science*. Vol 349: 1115-1120.

81. Mannion NM., Greenwood SM., Young R., Cox S., Brindle J., Read D., Nella C., Vesely C., Pontin CP., McLaughlin PJ., Jantsch MF., Dorin J., Adams IR., Scadden ADJ., Ohman M., Keegan LP., O'Connell MA. 2014. The RNA-editing enzyme ADAR1 controls innate immune responses to RNA. *Cell Reports*. Vol 9: 1482–1494.

82. Chung H., Calis JA., Wu X., Sun T., Yu Y., Sarbanes SL., Thi V., Shilvock AR., Hoffman H., Rosenberg BR., Rice CM. 2018. Human ADAR1 prevents endogenous RNA from triggering translational shutdown. *Cell* Vol 172: 811–824.

83. Rice GI., del Toro Duany Y., Jenkinson EM., Forte GMA., Anderson BH., Ariaudo G., Bader-Meunier B., Baildam EM., Battini R., Beresford MW., Casarano M., Chouchane M., Cimaz R., Collins AE., Cordiero NJV., Dale RC., Davidson JE., De Waele L., Desuerre I., Faivre L., Fazzi E., Isidor B., Lagae L., Latchman AR., Lebon P., Li C., Livingston JH., Lourenco CM., Margherita M., Masurel-Paulet A., McInnes IB., Menezes MP., Mignot C., O'Sullivan J., Orcesi S., Picco P., Riva E., Robinson RA., Rodriguesz D., Salvatici E., Scott C., Szybowaska M., Tolmie JL., Vanderver A., Vanhulle C., Vieira JP., Webb K., Whitney RN., Williams SG., Wolfe LA., Zuberi SM., Hur S., Crow YJ. 2014. Gain-of-function mutations in IFIH1 cause a spectrum of human disease phenotypes associated with upregulated type I interferon signaling. *Nature Genetics*. Vol 46: 503-510.

84. Ahmad S., Mu X., Yang F., Greenwald E., Park JW., Jacob E., Zhang C., Hur S. 2018. Breaching self-tolerance to Alu duplex RNA underlies MDA5-mediated inflammation. *Cell.* Vol 172: 797–810.

85. Cerritelli SM., Crouch RJ. 2009. Ribonuclease H: the enzymes in eukaryotes. *FEBS J.* Vol 276: 1494–1505.

86. Crow YJ., Leitch A., Hayward BE., Garner A., Parmar R. Griffith E., Ali M., Semple C., Aicardi J., Babul-Hirji R., Baumann C., Baxter P., Bertini E., Chandler KE., Chtayat D., Cau D., Dery C., Fazzi E., Goizet C., King MD., Klepper J., Lacombe D., Lanzi G., Lyall H., Martinez ML., Mathieu M., McKeown C., Monier A., Oade Y., Quarrell OW., Rittey CD., Rogers RC., Sanchis A., Stephenson JBP., Tacke U., Till M., Tolmie JL., Tomlin P., Voit T., Weschke B., Woods CG., Lebon P., Bonthron DT., Ponting CT., Jackson AP. 2006. Mutations in genes encoding ribonuclease H2 subunits cause Aicardi-Goutie`res syndrome and mimic congenital viral brain infection. *Nature Genetics*. Vol 38: 910-916.

87. Reijns M., Rabe B., Rigbe RE., Mill P., Astell KR., Lettice LA., Boyle S., Leitch A., Keighren M., Kilanowki F., Devenney PS., Sexton D., Grimes G., Holt IJ., Hill RE., Taylor MS., Lawson KA., Dorin JR., Jackson AP. 2012.Enzymatic removal of

ribonucleotides from DNA is essential for mammalian genome integrity and development. *Cell.* Vol 149: 1008–1022.

88. Hiller B., Achleitner M., Glage S., Naumann R., Behrendt R., Roers A. 2012. Mammalian RNase H2 removes ribonucleotides from DNA to maintain genome integrity. *The Journal of Experimental Medicine*. Vol 209: 1419-1426.

89. McElhinny SAN., Watts BE., Kumar D., Watt DL., Lundström E., Burgers PMJ., Johansson E., Chabes A., Kunkel TA. 2010. Abundant ribonucleotide incorporation into DNA by yeast replicative polymerases. *PNAS.* Vol. 107: 4949–4954.

90. Chon H., Vassilev A., DePamphilis ML., Zhao Y., Zhang J., Burgers PM., Crouch RJ., Cerritelli SM. 2009. Contributions of the two accessory subunits, RNASEH2B and RNASEH2C, to the activity and properties of the human RNase H2 complex. *Nucleic Acids Research.* Vol 37: 96–110.

91. Figiel M., Chon H., Cerritelli SM., Cybulska M., Crouch RJ. 2011. The structural and biochemical characterization of human RNase H2 complex reveals the molecular basis for substrate recognition and Aicardi-Goutières syndrome defects. *The Journal of Biological Chemistry*. Vol 286: 10540-10550.

92. Reijns MA., Bubeck D., Gibson LCD., Graham SC., Baillie GS., Jones EY., Jackson AP. 2011. The structure of the human RNase H2 complex defines key interaction interfaces relevant to enzyme function and human disease. *The Journal of Biological Chemistry*. Vol 286: 10530-10539.

93. Rohman MS., Koga Y., Takano K., Chon H., Crouch RJ., Kanaya S. 2008. Effect of the disease-causing mutations identified in human ribonuclease (RNase) H2 on the activities and stabilities of yeast RNase H2 and archaeal RNase HII. *FEBS Journal.* Vol 275: 4836–4849.

94. Chon H., Sparks JL., Rychlik M., Nowotny M., Burgers PM., Crouch RJ., Cerritelli SM. 2013. RNase H2 roles in genome integrity revealed by unlinking its activities. *Nucleic Acids Research.* Vol 41: 3130–3143.

95. Coffin SR., Hollis T., Perrino FW. 2011. Functional consequences of the RNase H2A subunit mutations that cause Aicardi-Goutières syndrome. *The Journal of Biological Chemistry.* Vol 286: 16984–16991.

96. Hasan M., Koch J., Rakhej D., Pattnaik AK., Brugarolas J., Dozmorov I., Levine B., Wakeland EK., Lee-Kirsch MA., Yan N. 2013. Trex1 regulates lysosomal biogenesis and interferon-independent activation of antiviral genes. *Nature Immunology*. Vol 14: 61-71.

97. Rehwinkel J., Maelfait J., Bridgeman A., Rigby R., Hayward B., Liberatore RA., Bieniasz PD., Towers GJ., Moita LF., Crow YJ., Bonthron DT., Reis e Sousa C. 2013. SAMHD1-dependent retroviral control and escape in mice. *The EMBO Journal* Vol 32: 2454–2462.

98. Diamond MS., Farzan M. 2013. The broad-spectrum antiviral functions of IFIT and IFITM proteins. *Nature Reviews Immunology.* Vol 13: 46-57.

99. Lazear HM., Lancaster A., Wilkins C., Suthar MS., Huang A., Vick SC., Clepper L., Thackray L., Brassil MM., Virgin HW., Nikolich-Zugich J., Moses AV., Gale MJ., Fruh K., Diamond MS. 2013. IRF-3, IRF-5, and IRF-7 coordinately regulate the type I IFN response in myeloid dendritic cells downstream of MAVS signaling. *PLOS Pathogens*. Vol 9: 1-15.

100. Mankan AK., Schmidt T., Chauhan D., Goldeck M., Honing K., Gaidt M., Kubarenko AV., Andreeva L., Hopfner K., Hornung V. 2014. Cytosolic RNA:DNA hybrids activate the cGAS–STING axis. *The EMBO Journal* Vol 33: 2938-2946.

101. Volkman HE., Stetson DB. 2014. The enemy within: endogenous retroelements and autoimmune disease. *Nature Immunology*. Vol 15: 415-422.

102. Lim YW., Sanz LA., Xu X., Hartono SR., Chedin F. 2015. Genome-wide DNA hypomethylation and RNA:DNA hybrid accumulation in Aicardi–Goutières syndrome. *eLife*. Vol 4.

103. Husebye H., Halaas Ø., Stenmark H., Tunheim G.,Sandanger Ø., Bogen B., Brech A., Latz E., Espevik T. 2006. Endocytic pathways regulate Toll-like receptor 4 signaling and link innate and adaptive immunity. *The EMBO Journal.* Vol 25: 683–692.

104. Liu Y., Jesus AA., Marrero B., Yang D., Ramsey SE., Montealegre Sanchez GA., Tenbrock K., Wittkowski H., Jones OY., Kuehn HS., Lee CR., DiMattia MA., Cowen EW., Gonzalez B., Palmer I., DiGiovanna JJ., Biancotto A., Kim H., Tsai WL., Trier AM., Huang Y., Stone DL., Hill S., Kim HJ., Hilaire C., Gurprasad S., Plass N., Chapelle D., Horkayne-Szakaly I., Foell D., Barysenka A., Candotti F., Holland SM., Hughes JD., Mehmet H., Issekutz AC., Raffeld M., McElwee J., Fontana JR., Minniti CP., Moir S., Kastner DL., Gadina M., Steven AC., Wingfield PT., Brooks SR., Rosenzweig SD., Fleisher TA., Deng Z., Boehm M., Paller AS., Goldbach-Mansky R. 2014. Activated STING in a vascular and pulmonary syndrome. *The New England Journal of Medicine.* Vol 371: 507- 518.

105. Xia T., Konno H., Ahn J., Barber GN.2016. Deregulation of STING signaling in colorectal carcinoma constrains DNA damage responses and correlates with tumorigenesis. *Cell Reports.* Vol 14: 282–297.

106. Lau L., Gray EE., Brunette RL., Stetson DB. 2015. DNA tumor virus oncogenes antagonize the cGAS-STING DNA-sensing pathway. *Science*. Vol 350: 568-571.

107. Moretti J., Roy S., Bozec D., Martinez J., Chapman JR., Ueberheide B., Lamming DW., Chen ZJ., Horng T., Yeretssian G., Green DR., Blander M. 2017. STING senses microbial viability to orchestrate stress-mediated autophagy of the endoplasmic reticulum. *Cell* Vol 171: 809–823.

108. Fink SL., Jayewickreme TR., Molony RD., Iwawaki T., Landis CS., Lindenbach BD., Iwasaki A. 2017. IRE1a promotes viral infection by conferring resistance to apoptosis. *Science Signaling*. Vol 10: 1-11.

109. Hur KY., So J., Ruda V., Frank-Kamenetsky M., Fitzgerald K., Koteliansky V., Iwawaki T., Glichmer LH., Lee A. 2012. IRE1a activation protects mice against acetaminophen-induced hepatotoxicity. *The Journal of Experimental Medicine.* Vol. 209: 307-318.

110. Kaser A., Lee A., Franke A., Glickman JN., Zeissig S., Tilg H., Nieuwenhuis E., Higgins DE., Schreiber S., Glichmer LH., Blumberg RS. 2008. XBP1 links ER stress to intestinal inflammation and confers genetic risk for human inflammatory bowel disease. *Cell.* Vol 134: 743–756.

111. Burns K., Clatworthy J., Martin L., Martinon F., Plumpton C., Maschera B., Lewis A., Ray K., Tschopp J., Volpe F. 2000. Tollip, a new component of the IL-1RI pathway, links IRAK to the IL-1 receptor. *Nature Cell Biology*. Vol 2: 346-351.

112. Zhang G., Ghosh S. Negative regulation of Toll-like receptor-mediated signaling by Tollip. *The Journal of Biological Chemistry.* Vol. 277: 7059–7065.

113. Didierlaurent A., Brissoni B., Velin D., Aebi N., Tardivel A., Kaslin E., Sirard JC., Angelov G., Tschopp J., Burns K. 2006. Tollip regulates proinflammatory responses to interleukin-1 and lipopolysaccharide. *Molecular and Cellular Biology*. Vol 2006: 735-742.

114. Hollien J., Weissman JS. 2006. Decay of endoplasmic reticulum-localized mRNAs during the unfolded protein response. *Science*. Vol 313: 104-107.

115. Pandol SJ., Gorelick FS., Gerloff A., Lugea A. 2010. Alcohol abuse, endoplasmic reticulum stress and pancreatitis. *Digestive Diseases.* Vol 28:776–782.

116. Jorgensen E., Stinson A., Shan L., Yang J., Gietl D., Albino AP. 2008. Cigarette smoke induces endoplasmic reticulum stress and the unfolded protein response in normal and malignant human lung cells. *BMC Cancer.* Vol 8: 1-30.

117. Lu Y., Cheng J., Chen L., Chaofei L., Chen G., Gui L., Shen B., Zhang Q. 2015.

Endoplasmic reticulum stress involved in high-fat diet and palmitic acid-induced vascular damages and fenofibrate intervention. *Biochemical and Biophysical Research Communications.* Vol 458: 1-7.

118. Mackenzie KJ., Carroll P., Lettice L., Tarnauskait Z., Reddy K., Dix F., Revuelta A., Abbondati E., Rigby RE., Rabe B., Kilanowski F., Grimes G., Fluteau A., Devenney PS., Hill RE., Reijns MA., Jackson AP. 2016. Ribonuclease H2 mutations induce a cGAS/STING dependent innate immune response. *The EMBO Journal.* Vol 35: 831-844.

119. Mackenzie KJ., Carroll P., Martin C., Murina O., Fluteau A., Simpson DJ., Olova N., Sutcliff H., Rainger JK., Leitch A., Osborn RT., Wheeler AP., Nowotny M., Gilbert N., Chandra T., Reijns MA., Jackson AP. 2017. cGAS surveillance of micronuclei links genome instability to innate immunity. *Nature*. Vol 548: 461-468.

120. Bartsch K., Knittler K., Borowski C., Rudnik S., Damme M., Aden K., Spehlmann ME., Frey N., Saftig P., Chalaris A., Rabe B. 2017. Absence of RNase H2 triggers generation of immunogenic micronuclei removed by autophagy. *Human Molecular Genetics*. Vol. 26: 3960–3972.

121. Raab M., Gentili M., de Belly H., Thiam H., Vargas P., Jimenez AJ., Lautenschlager F., Voituriez R., Lennon-Duménil AM., Manel N., Piel M. 2016. ESCRT III repairs nuclear envelope ruptures during cell migration to limit DNA damage and cell death. *Science*. Vol 352: 359-362.

122. Orzalli MH., Broekema NM., Diner BA., Hancks DC., Elde NC., Cristea IM., Knipe DM. 2015. cGAS-mediated stabilization of IFI16 promotes innate signaling during herpes simplex virus infection. *PNAS.* 1773–1781.

123. Vincent J., Adura C., Gao P., Luz A., Lama L., Asano Y., Okamoto R., Imaeda T., Aida J., Rothamel K., Gogakos T., Steinberg J., Reasoner S., Aso K., Tuschl T., Patel DJ., Glickman F., Ascano M. 2018. Small molecule inhibition of cGAS reduces interferon expression in primary macrophages from autoimmune mice. *Nature Communications.*Vol 8: 1-13.

124. Eckard SC., Rice GI., Fabre A., Badens C., Gray EE., Hartley JL., Crow YJ., Stetson DB. 2014. The SKIV2L RNA exosome limits activation of the RIG-I-like receptors. *Nature Immunology*. Vol 15: 839-846.

125. Glück S., Guey B., Gulen MF., Wolter K., Kang T., Schmacke N., Bridgeman A., Rehwinkel J., Zender L., Ablasser A. 2017. Innate immune sensing of cytosolic chromatin fragments through cGAS promotes senescence. *Nature Cell Biology.* Vol 19: 1061-1070.

126. Yang H., Wang H., Ren J., Chen Q., Chen ZJ. 2017. cGAS is essential for cellular senescence. *PNAS.* 4612–4620.

127. Hochrein H., Schlatter B., O'Keefe M., Wagner C., Schmitz F., Schiemann M., Bauer S., Suter M., Wagner H. 2004. Herpes simplex virus type-1 induces IFN production via Toll-like receptor 9-dependent and -independent pathways. *PNAS.* Vol 101: 11416–11421.

128. Ishikawa H., Barber GN. 2008. STING is an endoplasmic reticulum adaptor that facilitates innate immune signaling. *Nature.* Vol 455: 674-679.

129. Lu X., Zhao C., Zhang H., Yao X. 2017. iRhom2 is involved in lipopolysaccharide-induced cardiac injury in vivo and in vitro through regulating inflammation response. *Biomedicine & Pharmacotherapy.* Vol 86: 645–653.

130. O' Donnell K., An W., Schrum C., Wheelan SJ., Boeke JD. 2013. Controlled insertional mutagenesis using a LINE-1 (ORFeus) gene-trap mouse model. *PNAS.*

131. Choi JC., Hwang SY., Ahn K. 2018. Interplay between RNASEH2 and MOV10 controls LINE-1 retrotransposition. *Nucleic Acids Research* Vol 46: 1912–1926.

132. Liu N., Lee CH., Swigut T., Grow E., Gu B., Bassik MC., Wyoscka J. 2018. Selective silencing of euchromatic L1s revealed by genome-wide screens for L1 regulators. *Nature* Vol 553: 228-232.

133. Hetz C., Papa FR. 2017. The unfolded protein response and cell fate control. *Molecular Cell* Vol 69: 169-181.

134. Schoggins JW., MacDuff DA., Imanaka N., Gainey MD., Shrestha B., Eitson JL., Mar KB., Richardson B., Ratushny AV., Litvak V., Dabelic R., Manicassamy B., Aitchison JD., Aderem A., Elliott RM., Garcia Sastre A., Racaniello V., Snijer EJ., Yokoyama WM., Diamond MS., Virgin HW., Rice CM. 2013. Pan-viral specificity of IFN-induced genes reveals new roles for cGAS in innate immunity. *Nature* Vol 505: 691-695.

135. Lu K. Psakhye I., Jentsch S. 2014. Autophagic clearance of polyQ proteins mediated by ubiquitin-Atg8 adaptors of the conserved CUET protein family. *Cell* Vol 158: 549-563.

136. Olejniczak M., Urbanek MO., Krzyzosiak WJ. The role of the immune system in triplet repeat expansion diseases. *Mediators of Inflammation* Vol 2015: 1-11.

137. Farkash EA., Luning Prak ET. 2005. DNA damage and L1 retrotransposition. *Journal of Biomedicine and Biotechnology* Vol 2006: 1–8.

138. Chen K., Yuan R., Geng S., Zhang Y., Ran T., Kowalski E., Liu J., Li L. 2017. Toll-interacting protein deficiency promotes neurodegeneration via impeding autophagy completion in high-fat diet-fed ApoE mouse. *Brain, Behavior, and Immunity* Vol 59: 200-210.

139. Duennwald ML., Lindquist S. 2008. Impaired ERAD and ER stress are early and specific events in polyglutamine toxicity. *Genes and Development* Vol 22: 3308-3319.

140. Sliter DA., Martinez J., Hao L., Chen X., Sun N., Fischer TD., Burman JL., Li Y., Zhang Z., Narendra DP., Cai H., Borsche M., Klein C., Youle RJ. 2018. Parkin and PINK1 mitigate STING-induced inflammation. *Nature* Vol 561: 258-262.

141. Yang K., Huang R., Fujihira H., Suzuki T., Yan N. 2018. N-glycanase NGLY1 regulates mitochondrial homeostasis and inflammation through NRF1.*The Journal of Experimental Medicine* Vol 215.